2022-10-01

Post-rift geomorphological evolution of a passive continental margin (Paraiba region, northeastern Brazil): Insights from river profile and drainage divide analysis

Alves, FC

http://hdl.handle.net/10026.1/19955

10.1016/j.geomorph.2022.108384
Geomorphology
Elsevier

Title: Post-rift geomorphological evolution of a passive continental margin (Paraíba region, northeastern Brazil): Insights from river profile and drainage divide analysis

Authors: Fabio Corrêa Alves[a,b*], Martin Stokes[b], Sarah J. Boulton[b], Dilce de Fátima Rossetti[a], Márcio de Morisson Valeriano[a]

Authors address:

[a]Earth Observation and Geoinformatics Division, National Institute for Space Research, Av. dos Astronautas, 1758 - São José dos Campos -12245–970, São Paulo, Brazil (alves.fabioc@gmail.com; dilce.rossetti@inpe.br; marcio.valeriano@inpe.br)

[b]School of Geography, Earth and Environmental Sciences, Plymouth University, Devon PL4 8AA, UK (M.Stokes@plymouth.ac.uk; sarah.boulton@plymouth.ac.uk)

(*) corresponding author

1. Introduction

A passive margin is a transition zone between the oceanic and the continental lithosphere formed by rifting followed by seafloor spreading (Bradley, 2008). Low- and high-elevation passive margins have been commonly recognized (Gilchrist and Summerfield, 1990; Japsen et al., 2012). Low-elevation passive margins comprise coastal plains that gradually rise to low inland surfaces. High-elevation passive margins, also known as elevated passive continental margins (EPCMs), comprise high relief escarpments traversed by incised rivers that separate coastal plains from high inland plateaus (Gilchrist and Summerfield, 1990; Japsen et al., 2012). EPCMs are common in various bedrock lithologies, climatic conditions, and neotectonic settings, such as in west Greenland, southwest Africa, southeast Australia, Norway and northeast Brazil (Figure 1).

An assumption about EPCMs is that inland plateaus remain elevated after the main rifting, with minimal post-rift deposition (Gilchrist and Summerfield, 1990; Ollier and Pain, 1997; Gallagher et al., 1998). Elevated plateau persistence along EPCMs has been explained by lithospheric response to differential denudation between coastal and inland flanks due to isostasy (e.g., Gilchrist and Summerfield, 1990). However, the integration of offshore and onshore stratigraphic records with long-term denudation insights from thermochronology (Cobbold et al., 2001; Japsen et al., 2012 and references therein) suggests that EPCMs have multiple episodes of uplift, erosion and subsidence long after rifting. Thus, they are not necessarily permanent topographic highs. Conversely, short-term EPCM denudation histories using cosmogenic and/or geomorphological techniques indicate that erosion rates are low (i.e., a few tens of meters per million years), suggesting stability during the Late Cenozoic (Bierman and Caffee, 2001). In some margins, climate (Souza et al., 2019) or rock strength (Gallen, 2018) might be important controls of short-term EPCM erosional rates. However, the late stage evolution of passive margins is generally not well understood, especially along margins where cosmogenic data are limited or non-existent.

Potential new insights into passive margin development often include the morphology of the margin escarpment and plateau, especially in geologically data-poor regions. These landscape elements respond to changes in climatic (weathering) and base-level (surface / rock uplift, eustasy) boundary conditions by controlling the rates and directions of river incision and drainage divide migration (Willett et al., 2014; Roy et al., 2015). Therefore, the investigation of rivers and their catchment drainage divides has the potential to provide models of margin development and reveal the controls of their morphological changes. Longitudinal profiles of bedrock rivers and their knickpoints provide information on landscape steady-state or transience (Kirby and

Whipple, 2012). Profile-derived metrics, such as the normalized steepness index – k_{sn}, may reflect spatial or temporal variations in rock uplift rates, rock strength or climate (e.g., orographic rainfall patterns; Wobus et al., 2006; Whipple et al., 2013). Recent methods to access divide migration (Willett et al., 2014) can further be used to identify lithological, tectonic or climatic signals in fluvial settings (Goren et al., 2014; Bernard et al., 2019; Zondervan et al., 2020). These geomorphological approaches, together with geological information, have contributed with investigations aiming the development of fluvial landscapes, especially in tectonically active regions (Snyder et al., 2000; Wobus et al., 2006; Kirby and Whipple, 2012; Willett et al., 2014). However, this approach is still scarce in EPCMs (Gallen et al., 2013).

This study is focused on the South American EPCM. Our interest was to investigate the northeast sector of this margin, a Brazilian region of low-rate tectonics (uplift rates of 0.1 mm/yr for the last ~122 ka: Pedoja et al., 2011), but with a long record of moderate magnitude earthquakes (i.e., 5.2 mb body-wave magnitude), as informed by instrumented records (Bezerra and Vita-Finzi, 2000, Bianchi et al., 2018; Figure 1). Geological evidence suggests variations in the post-rift (i.e., Neogene and Quaternary) tectonic styles and rates along this margin (Marques et al., 2014; Gandini et al., 2014; Nogueira et al., 2015; Vasconcelos et al., 2019; Bezerra et al., 2020). This is especially the case of the Paraíba region, the final bridge between the South American and African plates that remained active up to the Early Cretaceous (Matos, 1992). Notably, this region records an abundance of Quaternary deposits with seismically-triggered soft sediment deformation (Rossetti et al., 2011a, 2011b; Alves et al., 2019; Andrades Filho et al., 2021) and some uplifted marginal marine deposits (Gandini et al., 2014). These deposits suggest that the relief in the Paraíba region may have developed under tectonic instability. As a result, a transient fluvial landscape with drainage network reorganisation is expected, which might include incised bedrock channels, knickpoints, unstable and mobile drainage divides. The investigation of this fluvial landscape has the potential to inform on the geomorphological evolution of this and similar passive continental margins elsewhere.

We explored whether variations in tectonic uplift during the Quaternary promoted responses on transient fluvial landscape in the Paraíba region. This was achieved by searching: 1) the long river profile geometries based on the types and distribution of knickpoints, which allowed to explore spatial patterns and controls on base-level lowering (i.e., rock strength, uplift, eustasy, capture); 2) the k_{sn} values and their relationship with spatial variations in uplift rates and bedrock; 3) the fluvial incision, a proxy for surface uplift (Kirby and Whipple, 2012), as the rivers of the Paraíba region may have changed their incision dynamics due to shifts in the rates of tectonic uplift during the Quaternary; and 4) the mobility of the catchment drainage divides and the dynamics of divide migration, which were achieved by analyzing their potential relationship to variations in the tectonic uplift or spatial differences in bedrock erodibility.

2. Geological and geomorphological setting

2.1. The passive continental margin of northeastern Brazil

Northeastern Brazil shows two geographic trends of passive margin development formed during the Late Mesozoic breakup of Pangea: 1) an equatorial margin, with an E- to W-trending coast; and 2) an eastern margin with a ~ NNE- to SSW-trending coast (Figure 1). The eastern margin, focus of this study, is drained by NE-SW- or NW-SE-oriented rivers, such as the Paraíba River and lower course of the São Francisco River. Most rivers that drain this margin originate in highlands dominated by a complex of pre-rift Precambrian rocks (Almeida et al., 1981), bordered to the north and east/northeast by Cretaceous and Cenozoic deposits of the coastal lowlands (Figure 1). The relief changes gradually from the highlands to the coast and lacks a well-defined escarpment.

Figure 1.

The highlands with pre-rift Precambrian rocks are from the São Francisco Craton and Borborema Provinces (Almeida et al., 1981). These consist of Archean and Proterozoic rocks that separate the marginal sedimentary basins to the east from the intracratonic Paleozoic Parnaíba Basin to the west (Figure 1). The Borborema Province was built by the collision between the São Luis/West Africa and São Francisco/Congo cratons (West Gondwana amalgamation) during the Neoproterozoic Brasiliano/Pan-African orogeny (Almeida et al., 1981). These cratonic areas are formed by crystalline basement rocks of variable strengths (Almeida et al., 1981; Brito Neves et al., 2004).

The passive continental margin of northeastern Brazil formed during the Triassic-Jurassic to Early Cretaceous rifting between the South American and African continents, which culminated with the opening of the South Atlantic Ocean (Matos, 1992). This event resulted in several sedimentary basins along the coast in both the marine and continental realms (Figure 1). The Paraíba Basin is one of these basins, representing the last continental bridge between the South American and African plates (Matos, 1992). This basin was filled during the rifting and the post-rifting (Rossetti et al., 2012). The rift deposition occurred in the Late Cretaceous and is recorded by sandstones of the Beberibe Formation, limestones and calciferous sandstones of the Itamaracá Formation, and limestones of the Gramame Formation (Barbosa et al., 2003). The post-rift stage is recorded by siliciclastic deposits of Miocene and Late Quaternary ages, and corresponds to the Barreiras Formation and Post-Barreiras Sediments (Barbosa et al., 2003; Rossetti et al., 2012). All these units are delimited by regional unconformities. The unconformity between the Cretaceous and Neogene units are particularly prominent, being marked by an erosional surface with a deep lateritic paleosol horizon (Rossetti et al., 2012, 2013). This unconformity was formed during a prolonged time of tectonic stability. Fault reactivation during the Neogene and Quaternary (i.e., late post rift stage) created new space for sediment accommodation, which was filled by the deposits of the Barreiras Formation and Post-Barreiras Sediments (Rossetti et al., 2012). These deposits show evidence of syn-sedimentary tectonic deformation, which indicates that the region remained tectonically unstable even after the main rifting (Rossetti et al., 2011b).

The Paraíba Basin is bounded by two major tectonic structures, the Pernambuco Shear Zone to the south and the Mamanguape Fault, the latter a branch of the Patos Shear Zone to the north (Figure 1). These shear zones formed during the Neoproterozoic Brasiliano/Pan-African orogens (Almeida et al., 1981; Bezerra et al., 2011) and constitute prominent continental-scale Precambrian basement structures (Figure 1). They are E-W- and ENE-WSW-oriented shear zones, 1 to 5 km in width, and hundreds of kilometers in length. The present-day instrumented earthquake records show a considerable number of low to moderate earthquake magnitudes (up to 6.0 mR) near some shear zones, such as the Pernambuco Shear Zone, and in other areas of the northeastern Brazilian margin (Figure 1; Bezerra and Vita-Finzi, 2000; Bianchi et al., 2018).

The pre-existing shear zones in this passive continental margin were reactivated during the rift stage and controlled the location, geometry and sedimentary fill of the marginal basins (e.g., Matos, 1992; Bezerra et al., 2011; 2014). Reactivations occurred also in the post-rift phase (Neogene and Quaternary), when basin bounding faults were displaced by strike-slip transpressive stress in concert with regional stress field changes, which caused basin inversions (e.g., Araripe, Rio do Peixe and Potiguar basins; Marques et al., 2014; Nogueira et al., 2015; Bezerra et al., 2020). However, the northeastern Brazilian margin also records a set of ~ NE-SW-striking normal faults, consistent with evolution models of transtensional strike-slip fault systems (e.g., Bezerra et al., 2014, 2020). These normal faults serve as pathways for watersheds that link the highlands to the Atlantic Ocean.

2.2. Geomorphology of the study area

Our study focuses a 165-km long and 132-km wide EPCM located in the Paraíba region (Figures 1 and 2a). From north to south, ocean-facing catchments in this margin are formed by large and generally SW- to NE-oriented trunk streams, such as the Curimataú, Camaratuba, Mamanguape, Miriri and low Paraíba rivers (Figure 2a). These rivers form wide valleys, filled in the downstream sectors by late Holocene alluvial sediments (Figure 2a). Trunk streams are fed by NNW-SSE or NE-SW oriented tributaries (Figure 3) that extend from the highlands to the coastal plains. These tributaries are mainly bedrock rivers with thin alluvial deposits downstream. Many tributaries of the Paraíba River are disrupted by normal faults of the Cariatá Graben to the south (cf. Brito Neves et al., 2004; Bezerra et al., 2008). This is an asymmetrical trough of ~ 40 km long, ~ 25 km wide, and 250–550 m deep (Bezerra et al., 2008). Two main fault reactivation events of pre-Late Pleistocene and Late Pleistocene ages controlled the development of this graben (Bezerra et al., 2008). To the north, tributaries of the Mamanguape River are disrupted by the Patos Shear Zone, where the tectonic effect is still poorly known (Figure 3).

Figure 2.

Figure 3.

The regional drainage divide bounds catchments to the west, some 140 km from the coast (Figures 2a and 3) within the highland plateau. The plateau stands at altitudes averaging 750 m a.s.l., and it is constituted by Precambrian crystalline basement rocks (e.g., gneisses, migmatites, schists, and granites), and secondarily Paleogene sandstones from the Serra do Martins Formation (Morais Neto et al., 2008; Figure 2a). A deeply dissected low elevation (< 200 m a.s.l.) surface, known as Sertaneja Depression (Costa et al., 2020), occurs to the east of this plateau (Figure 2b). The low topography of this depression is locally interrupted by Cretaceous igneous rocks that stands at altitudes up to 600 m (Figure 2a). The coastal lowlands are dominated by Miocene (Barreiras Formation) and Late Quaternary (Post-Barreiras Formation) siliciclastic deposits (Rossetti et al., 2012), and secondarily Late Cretaceous sandstones and limestones (Barbosa et al., 2003; Figure 2a). The Barreiras Formation, first attributed to essentially continental environments, were reinterpreted as having deposits formed in various coastal, mainly estuarine environments (see Rossetti et al. 2013 for a review). The Post-Barreiras Sediments (Rossetti et al., 2012) include two informal stratigraphic units dated from the Late Pleistocene (Post-Barreiras 1 – PB1) and early/middle Holocene (Post-Barreiras 2 - PB2). PB1 consists of sandstones interbedded with mudstones and conglomerates, formed by marine (Gandini et al., 2014) or alluvial (fluvial and gravitational) processes (Rossetti et al., 2012). PB2 is constituted by friable and massive, mostly aeolian sands (Rossetti et al., 2012). Both the Miocene and Late Quaternary deposits discordantly overly Precambrian units. The coastal lowlands consist of a table-shaped relief (Costa et al., 2020) and a domal relief (Alves et al., 2019; Figure 2a-b), which give way to an adjacent narrow coastal plain to the east.

The climate in the Paraíba region is currently humid tropical in the coast, with an average annual precipitation of 1917 mm and an average temperature of 26.5 °C (Carvalho et al., 2020). A semi-arid climate with prolonged droughts prevails inland. The paleoclimate in this region remains elusive, but successive planation (erosional) surfaces have long been related to prevailing semi-arid conditions (King, 1967). However, studies based on new methodologies, such as apatite fission track, cosmogenic nuclides and remote sensing, disagree that climate has played a main role in defining the landscape of this passive margin, and suggest instead a main neotectonic control (Bezerra et al., 2008; Japsen et al., 2012; Gandini et al., 2014; Alves et al., 2019 and references therein).

3. Methods

We used a digital elevation model (DEM) for the geomorphological analysis of tributary stream profiles and catchment drainage divides to investigate tectonic uplift-induced base-level changes and drainage network reorganization during the Quaternary of the Paraíba passive margin.

3.1. DEM processing

The study area was assessed using the 30-m spatial resolution Shuttle Radar Topography Mission (SRTM) DEM derived from C-band interferometric synthetic aperture radar (InSAR) techniques (Farr et al., 2007). This product has greater ability to reveal surface information than other DEMs (e.g., Boulton and Stokes, 2018), since the C-band (~ 5.6 cm) can penetrate through the dense clouds and the upper tree canopy, typical in tropical regions (Henderson and Lewis, 1998) as in the case of the study area. This DEM was filled using minimum topographic values from surrounding pixels to generate a continuous drainage network. The processed DEM was used as the basis to extract long river profiles and topographic metrics of drainage divides using codes available in ChiProfiler (Gallen and Wegmann, 2017), Topographic Analysis Kit (TAK, Forte and Whipple, 2019) and DivideTools (Forte and Whipple, 2018). All these codes are based on functions of TopoToolbox (Schwanghart and Scherler, 2014).

3.2. River profile analysis

A long profile is a plot of river channel elevation against distance (Hack, 1957). The geometry of long river profiles and the derivation of fluvial metrics have been regularly used in geomorphological research to assess rates of relative base-level fall due to variations in tectonics, river capture, sea-level, climate, or lithology (Wobus et al., 2006; Kirby and Whipple, 2012). This approach can benefit geomorphic investigations of bedrock rivers in landscapes where the extent and/or the scarcity of geological exposures make field-based investigations difficult, such as in the study area.

River profiles were extracted from the drainage network using routine DEM techniques (e.g., flow direction and flow accumulation). A drainage area threshold (A_{cr}) of 1 km² or higher was applied to the drainage network to eliminate upstream river segments related with debris-flow processes (Wobus et al., 2006; Kirby and Whipple, 2012). The river profile analysis was applied to 43 tributary streams (Figure 3) of third or higher orders (cf., Strahler, 1957). These orders were chosen because they are often characterized by bedrock segments, as required for detachment-limited models of erosion (Kirby and Whipple, 2012). The selected river tributaries flow across the elevated plateau and coastal lowlands, crossing a range of lithologies of varied ages and pre-existing structures.

The passive margin river profiles were analyzed using the stream power incision model (SPIM) (Kirby and Whipple, 2012; Lague, 2014). The generalized equation of the SPIM can be described by an empirical power law relationship (Hack, 1957; Kirby and Whipple, 2012) between channel slope (S) and upstream drainage area (A; a proxy for discharge):

$$S = k_s A^{-\theta} \tag{1}$$

where, k_s is the channel steepness index ($m^{2\theta}$); and θ the channel concavity index (dimensionless) (Snyder et al., 2000). In steady-state landscapes, where uplift equals erosion, spatial variability in k_s values may reflect spatial or temporal changes in erosion and uplifting rates in reliefs with homogeneous lithological and climatic conditions (Wobus et al., 2006; Kirby and Whipple, 2012). To compare k_s values from river profiles with different sizes, the normalized channel steepness index (k_{sn}) is obtained based on a fixed reference concavity (θ_{ref}) (Wobus et al., 2006). Empirical studies have shown that θ varies between 0.4–0.6, but a fixed reference concavity of 0.45 is often used for characterizing steady-state channels in a variety of reliefs across the world (e.g., Snyder et al., 2000; Wobus et al., 2006; Kirby and Whipple, 2012).

Parameters S and A can be extracted directly from DEMs, while k_{sn} and θ are extracted from the linear regression between S and A on a log-log graph. However, the channel slope may enhance significant scatter with direct influence on the k_{sn} calculation, since topographic data comprise noisy variations (microrelief, artifacts and errors) that are propagated to the slope (first order derivative of elevation). To circumvent these issues and extract more reliable k_{sn} values, the integral method (integration of drainage area along flow distance) has been proposed (Perron and Royden, 2013). This approach rearranges equation 1 by replacing S for dz/dx, where dz is the elevation change and dx the distance along the channel. The integration is performed in an upstream direction from a base-level (x_b) to a given point along the channel (x) as follows:

$$z(x) = z(x_b) + \left(\frac{ks}{{A_0}^{\theta}}\right) \int_{x_b}^{x} \left(\frac{A_0}{A(x)}\right)^{\theta} dx \qquad (2)$$

with the variable

$$\chi = \int_{x_b}^{x} \left(\frac{A_0}{A(x)}\right)^{\theta} dx \qquad (3)$$

where, A_0 refers to a reference drainage area inserted to make the area term dimensionless (c.f., Perron and Royden, 2013). Assuming steady-state landscapes, with invariant bedrock erodibility, the longitudinal coordinate χ with dimensions of length has a linear relationship with elevation $z(x)$ (Perron and Royden, 2013; Willett et al., 2014; Whipple et al., 2017). In this situation, a given profile will appear as a straight line in the χ-elevation space (also known as chi plot).

The k_{sn} calculation was performed using the integral method to identify regions in the passive margin with spatial or temporal variability in rock uplift rates, climate or differences in bedrock erodibility. The integral method was calculated using an A_0 of 1 m^2 to ensure that the local slope of a transformed profile is the k_{sn} (Perron and Royden, 2013; Gallen and Wegmann, 2017). Exploratory analysis of log-log slope-area plots of tributaries with graded stream profiles (concave shapes) in the study area revealed an average concavity value of 0.41 (Supplementary Figure S1). This value, which is very close to the standard concavity value of 0.45 (Wobus et al., 2006; Kirby and Whipple, 2012) was used in this study as basis to calculate the k_{sn} and allowed us to make comparisons with previous works carried out in other similar EPCMs (Gallen, 2018; Souza et al., 2019) and Brazilian intracontinental (Peifer et al., 2021) settings. Average

k_{sn} values were calculated for the tributaries by adjusting linear regression bounds in profile segments above and below knickpoints; and for the entire drainage network using stream segment lengths of 1 km, since k_{sn} values are strongly variable over short distances.

The potential influence of rock strength on the spatial variability/magnitude of k_{sn} values was investigated by averaging the k_{sn} of drainage network by rock types. In the absence of other parameters (e.g., quantitative *in situ* rock mass strength, jointing, and weathering data; Bursztyn et al., 2015), the average k_{sn} considers only the lithological character of rocks (Bernard et al., 2019; Zondervan et al., 2020) and can be used as a proxy for bedrock erodibility (Gallen, 2018). In this study, the various geological units were simplified into a smaller number of lithological groups (Supplementary Figure S2). According to literature-based descriptions of rock strength (e.g., Goudie, 2006), we defined three major rock groups in terms of relative importance of resistance to fluvial erosion using the official geological map from the Brazilian Geological Survey (CPRM) at 1:1000000 scale (http://geosgb.cprm.gov.br/geosgb): (i) low resistant sedimentary rocks; (ii) moderately resistant metamorphosed rocks; and (iii) highly resistant igneous and meta-igneous rock units (Table 1; Figure 6). The average and standard deviation k_{sn} were extracted for each rock group based on a total of 10,000 random samples. These samples were distributed proportionally to the area of each group based on their uneven distribution in the studied passive margin (sedimentary rocks = 25.4 %; metamorphosed sediments = 5.3 %, and igneous and meta-igneous rocks = 69.3 %). This analysis was not applied to the alluvial/marine/aeolian deposits to avoid abrupt changes in k_{sn} related to depositional channel segments.

Table 1.

In addition to the k_{sn} approach, rivers under non-steady-state conditions (uplift ≠ erosion) may produce unbalanced geomorphic features (transient features), such as convex-upward discontinuities (knickpoints; Kirby and Whipple, 2012). The study of knickpoints along river profiles has been used as an indicator of rivers with a transient response due to rock strength controls or perturbations related to relative base-level changes. These are caused by tectonics (e.g., increase in the fault slip rates), river capture, sea-level fall and/or climatic variations. These factors can enhance or reduce the efficiency of river incision (Kirby and Whipple, 2012; Whipple et al., 2013). We identified major knickpoints by visual interpretation of convex-upward deviations in river profile shapes from the distance-elevation and χ-elevation plots. Knickpoints were classified into two end-member morphologies, vertical-step or slope-break (c.f., Haviv et al., 2010 and Whipple et al., 2013), based on the recognition of spikes and breaks in log-log slope-area graphs, respectively. Given the importance of knickpoints in preserving information about the tectonic evolution of fluvial landscapes (Kirby and Whipple, 2012), they were further characterized in terms of: spatial patterns between the knickpoint locations and lithological contacts/pre-existing basement structures, distribution pattern, statistical relationships, formation and behavior.

The knickpoint analysis also included the application of two statistical hypothesis tests: the unpaired two-samples T-test (parametric test); and the Mann-Whitney U test (non-parametric test) (c.f., Noether, 1991; Venables and Smith, 2002). These tests aimed to examine two clusters of knickpoints in the study area. To attend the T-test assumptions, data normality analysis using the Shapiro-Wilk test and homogeneity of variances based on Levene's test were required (Venables and Smith, 2002). The parameters elevation, slope, relative relief and k_{sn} at a given knickpoint were chosen because they may inform important aspects about the knickpoint origin and, ultimately, the passive margin evolution. The relative relief was calculated varying the moving window radius (1, 3 and 5 km) to assess the windows sensitivity. Only the attributes that failed in the normality analysis (T-test) were submitted to the Mann-Whitney U test. The following null (h_0) and alternative (h_a) hypotheses were defined assuming a significance level (α) of 0.05: h_0 = the means/medians of the two groups of knickpoints are the same; h_a = the means/medians of the two groups of knickpoints are different.

The amount of fluvial incision was calculated for tributaries with slope-break knickpoints. Fluvial incision was estimated from the reconstruction of channel profiles, an approach typically applied to access the uplift history of a given area (Kirby and Whipple, 2012). The calculations were made downstream of the slope-break knickpoints in the lower reaches of the studied tributaries, that is, the region potentially adjusting to perturbations. Following the method implemented in the TAK (Forte and Whipple, 2019), the river profiles downstream of the knickpoints were projected using linear least squares fitting on the χ-elevation relationship, with a confidence interval of 95%. The estimated fluvial incision was then obtained by subtracting the elevations from the projected (relict channel profile) and present-day profiles at the fault. The position of the fault at the profile was defined based on the visual interpretation of river locations and major morphostructural lineaments/faults/shear zones in the study area. The lineaments (204 in total with a main NE-SW trend) were mapped using SRTM-based shaded relief representations in different azimuth angles at a fixed 1:100.000 scale (Supplementary Figure S3). Known faults and shear zones were derived from previous publications (Bezerra et al., 2008, 2014).

3.3. Assessment of divide mobility

Landscapes undergoing transient adjustments due to changes in boundary conditions, such as those recording incised rivers, knickpoints and contrasting erosion rates between adjacent drainage basins, may show drainage divide migration (Willett et al., 2014). Active drainage divide migration has been recognized in a variety of fluvial landscapes as a result of many competing controls, such as lithology, where the drainage divide moves towards highly resistant rocks (Bernard et al., 2019; Zondervan et al., 2020), the spatial variability of precipitation (Goren et al., 2014), asymmetric tectonic uplift (He et al., 2019), or large discrete river capture (Willett et al., 2014; Whipple et al., 2017).

The assessment of divide mobility has been performed by maps of the drainage network coloured by χ (χ-maps). Significant variations in χ on opposite sides of a drainage divide (χ-anomalies) may suggest divide migration (e.g., due to a river capture), which is driven by differences in erosion rates of river channels (Willett et al., 2014). Alternatively, it has been suggested that divide instability analysis can be made more reliable by interpreting cross-divide differences using topographic metrics, also known as Gilbert metrics (i.e., elevation at the channel head, upstream relative relief and upstream gradient), as these are topographic proxies for erosion rates (Whipple et al., 2017; Forte and Whipple, 2018). In this study, the stability/mobility and direction of divide migration were investigated through the χ-map and Gilbert metrics extracted at the channel heads. The χ-map was generated for complete drainage basins with outlets $\geq$ 1 m a.s.l. based on the SRTM-DEM. For the sake of simplification, we analyzed only the drainage divides bounding major transverse fluvial systems. The drainage divide was assumed to be stable if the mean on one side of the divide overlaps the uncertainty of the mean on the opposite side; otherwise, the divide was assumed as mobile (c.f., Forte and Whipple, 2018). The direction of divide migration was defined following the interpretations described in Willett et al. (2014), Whipple et al. (2017) and Forte and Whipple (2018).

4. River profiles and drainage divides

4.1. Knickpoints, k_{sn} and fluvial incision

The Paraíba region has tributaries up to ~117 km long and catchment areas up to ~994 km² (Figure 3). Tributary streams crossing the Precambrian highlands are longer than those from the coastal lowlands (average lengths of ~34 km and 24 km, respectively). These tributaries showed river profiles that can be qualitatively classified into two major groups according to their profile shapes shown in distance-elevation and χ-elevation plots: (i) relatively graded profiles (concave-up profiles and linear χ-profiles); and (ii) ungraded profiles (convex-up river profiles and non-linear χ-profiles; Figures 4a-f and 5a-f).

Figure 4.

Figure 5.

The first group of graded profiles comprises twenty-one tributaries, recorded mostly in the low-lying terrains of the passive margin, with profile elevations not exceeding 450 m a.s.l. (Figure 4a-f). These profiles have no knickpoints. Some small tributaries on flat terrains capped by Miocene deposits in the southeast sector of the study area show river profiles with convex segments, suggesting broader knickzones (rivers 26, 27, 28, and 29 in Figure 4f). However, these tributaries did not show clearly recognizable breaks or spikes in the log-log slope-area plots.

The second group of ungraded profiles is represented by twenty-two tributaries (Figure 5a-f). These were recorded mainly in the Precambrian highlands of the passive continental margin to the west, and secondarily, in the coastal lowlands to the east. They showed: profile elevations up to 700 m a.s.l. (Table 2); and river profiles with widely scattered knickpoints (vertical-step and slope-break; Figure 5a-i).

Table 2.

We recorded a total of fourteen vertical-step knickpoints (green dots in Figure 5a-i). They occurred at or close to lithological contacts between Precambrian units (e.g., knickpoints from rivers 1, 2, 5, 13 and 15 in Figure 6a and Supplementary Figure S4); and in river segments downstream of slope-break knickpoints. These knickpoints occurred at elevations between 73 and 507 m a.s.l., and revealed maximum k_{sn} values almost twice as high as the slope-break knickpoints (Table 2). For instance, vertical-step knickpoints showed an average k_{sn} at knickpoint of 38.5 $m^{0.9}$ and a maximum k_{sn} value of 85.3 $m^{0.9}$, while slope-break knickpoints displayed an average k_{sn} at knickpoint of 27.4 $m^{0.9}$ and a maximum k_{sn} value of 49.3 $m^{0.9}$ (Table 2).

Figure 6.

The majority of the knickpoints were classified as slope-break type (purple dots in Figure 5). They occurred across a range of elevations (65-676 m a.s.l.) and were limited by downstream segments steeper than upstream (see k_{sn} ratio in Table 2). Most rivers had one slope-break knickpoint each, but three rivers (rivers 5, 6, and 14) exhibited two slope-break knickpoints. Knickpoints from river 14 are likely to be part of a single knickpoint, as they showed a similar morphology and are located close to each other across a distance of ~5 km. The slope-break knickpoints occurred generally aligned across a ~ NNE-SSW-oriented belt over the highlands (Figure 6a), where they lie upstream of the Patos Shear Zone to the north and upstream of the normal faults bounding the Cariatá Graben to the south (Figure 7). However, a small number of knickpoints were also observed closer to lithological contacts of the Precambrian units or between these and Miocene-Quaternary deposits (e.g., knickpoints from rivers 2 and 10 in Figure 6a and Supplementary Figure S4). Only the current position of the slope-break knickpoints was recorded, but their behaviour is generally mobile over time (Crosby and Whipple, 2006; Berlin and Anderson, 2007; Boulton and Whittaker, 2009).

Figure 7.

The k_{sn} values ranged from 1 to 462 $m^{0.9}$ with a right-skewed distribution and an average k_{sn} of 15 $m^{0.9}$ (Figure 6a). Higher k_{sn} values (> 20 $m^{0.9}$) were found in the highlands (to the west) and dome-like reliefs (to the east), where the distribution of relative relief values is high (Supplementary Figure S5). Lower k_{sn} values (< 20 $m^{0.9}$) occurred mainly over the Precambrian low-lying and sedimentary table-like terrains. The rock group average k_{sn} analysis showed a trend of an increased slope of channels flowing over more resistant rock units (i.e., igneous and meta-igneous rocks of the Precambrian basement), in contrast to low steepness channels that drain over less resistant rock units (i.e., sedimentary rocks) (Figure 6b). Abrupt changes in k_{sn} values owing to local differences in bedrock resistances were evident in the northwest and northeast sectors of the study area, where pre-rift rock units of Precambrian age are in contact with Paleogene and Miocene-Quaternary deposits, respectively (Figure 6a). However, local changes in k_{sn} were detected even in bedrock terrains of relatively similar resistances, which cannot be explained only by lithological control. Furthermore, this analysis showed a low variability of k_{sn} values among different rock groups (Figure 6b and Supplementary Figure S2), in general ranging from 10 to 25 $m^{0.9}$, but with high uncertainties.

The distribution pattern of the knickpoints (slope-break and vertical-step) in the study area is shown in Figure 8a. K_{sn} values downstream of knickpoints were higher than upstream for both slope-break and vertical-step morphologies, but with higher uncertainties for the latter (Table 2). This situation was observed mainly for the tributary streams flowing over the Precambrian terrains of the study area, where knickpoint elevations are high (Figure 8a). The statistical analysis between k_{sn} and relative relief values at knickpoints showed moderate and weak positive linear relationships for the slope-break ($r^2 = 0.61$) and vertical-step ($r^2 = 0.36$) morphologies, respectively (black/white dots in Figure 8b). The high coefficient of determination for the slope-break knickpoints and their spatial correspondence with the structural fabric (i.e., upstream of known faults) of the study area suggest that they may have inherited some tectonic influence. Therefore, subsequent analyses were carried out based only on the slope-break knickpoints, given their potentially higher tectonic significance (Kirby and Whipple, 2012; Whipple et al., 2013).

Figure 8.

We carried out some statistical analysis using information from the knickpoints and their drainage basins to characterize the knickpoint formation (e.g., one or multiple knickpoint clusters) and behavior (i.e., anchored in place or mobile). The regression analysis of the knickpoint elevation versus drainage area, and the knickpoint elevation against the knickpoint distance from mouth showed weak relationships, with very poor determination coefficients ($r^2 < 0.13$) when the slope-break knickpoints were analyzed together (Figure 9a-b). In contrast, these relationships were strengthened when the knickpoints from the north (Patos Shear Zone region) and south (Cariatá Graben region) of the passive continental margin were analyzed individually. The northern and southern knickpoints showed positive ($r^2 = 0.43$ and 0.51) and negative ($r^2 = 0.42$ and 0.46) linear relationships, respectively (Figure 9a-b). The statistical analysis between the average basin gradient versus catchment area (not shown here) revealed a negative linear relationship, with a moderate determination coefficient ($r^2 = 0.42$) only for the basins located in the southern sector of the study area. These drainage basins have steeper gradients than those from the northern sector, especially the small basins located closer to the Cariatá Graben (Figure 7). The discrepancies with the knickpoint / drainage basin relationships and the high range of slope-break knickpoint elevations led us to test the hypothesis of two different clusters of knickpoints in the study area. The T-test showed that the means of the relative relief (radius of 3 and 5 km) of the southern knickpoints are statistically different from the means of the northern ones (p-value < 0.05; Table 3), assuming an α of 0.05. The Mann Whitney U test did not show any statistical differences in the slope of the knickpoints from both sectors (Table 3), although limitations of dataset size could be an issue.

Figure 9.

Table 3.

The knickpoint retreat distance from the mouths and the downstream distances from the drainage divides positively scaled with the total drainage area and drainage area below and above the slope-break knickpoints, with strong r^2 coefficients (i.e., $r^2 > 0.89$; Figure 9c-e). Knickpoints from larger basins (e.g., from rivers 5 and 14, see Table 2) travelled further upstream than knickpoints from smaller basins (e.g., from rivers 3, 4 and 20). The drainage area upstream of knickpoints ranged from 4.2 to 238.3 km² and from 2.4 to 125.3 km² for the northern and southern knickpoints, respectively. Hack's exponents varied from 0.60-0.68 when all the knickpoints are analysed together; 0.62-

0.77 for the northern knickpoints; and 0.56-0.58 for the southern knickpoints (Figure 9c-e).

The amounts of fluvial incision derived from river profile segments downstream of slope-break knickpoints were 140 m on average (Table 2). Average fluvial incision was 156 m for tributaries over the Precambrian highlands and 43 m for tributaries crossing the coastal lowlands. This situation suggests spatially variable fluvial incision in the studied region, with higher incision amounts inland towards the elevated plateau formed by pre-rift Precambrian basement rocks.

4.2. Drainage divide and divide mobility

The main drainage divides of the study area extend from the elevated plateau to the coastal lowlands, a total of 480 km in length (Figure 10a). In general, the drainage divides have either NE-SW- or NW-SE-oriented segments and are at a maximum 125 km from the coastline. These were qualitatively divided into divide segments (D1-D8) to assess local variations in divide migration (Figure 10a). From west to east, the drainage divide segments traversed a range of lithologies (i.e., pre-rift basement rocks and post-rift depositional sequences) with contrasting erodibilities (Figures 2a and 10a). The longest drainage divide segment (D5) is 153 km long and runs from 740 m a.s.l. across high resistant Precambrian units (igneous and meta-igneous rocks) and, secondarily, low resistant Paleogene deposits to the west. Divide D5 decreased in elevation to ~ 350 m a.s.l., as it crossed moderate resistant metamorphic rocks to the east. Divide D1 to the southwest crosses only high resistant Precambrian units, with elevations ranging from ~ 500 to 140 m a.s.l. Divides D2-D3-D4 and D6-D7 to the southeast and northeast, respectively, occur between high to moderate resistant Precambrian units and low resistant to erodible Miocene to Quaternary-deposits. D8 also crosses deposits formed since Miocene, but it occurs on domal reliefs with elevations up to 200 m a.s.l.

Figure 10.

Most divide segments (i.e., D1, D4, D5, D6 and D7) were stable, with no significant cross-divide differences in the χ-map and Gilbert metrics (Figures 10a and 11a-d). For instance, D1, D4, D6, and D7 showed relatively equal average channel elevation values of about 100 m a.s.l. (Figure 11a). They also displayed similar hillslope gradient values around 0.1 and relative relief values ranging from 40 to 50 m (Figure 11b-c). D5 showed the highest average elevation value up to 500 m a.s.l., the highest mean hillslope gradient, and relative relief of approximately 0.15 and 75 m, respectively (Figure 11a-b-c).

Figure 11.

Among the drainage divide segments, only three (D2, D3, and D8; Figures 10a and 11a-d) showed variations in χ and Gilbert metrics on both sides of the divide, indicating divide migration. D8, located in a coastal lowland dome, had differences only in the Gilbert metrics of hillslope gradient and relative relief. It also had the highest average hillslope gradient and relative relief values (0.15 and 75 m, respectively), with northward divide motion (Figure 11b-c-d). D2 and D3, located to the southeast, revealed differences in both χ and Gilbert metrics, with relatively similar topographic metrics (average channel elevation of ~ 100 m; hillslope gradient of ~ 0.05; relative relief of ~ 50 m; Figure 11a-c). χ and Gilbert metrics suggest divide movement to the southeast for D2 and to the northeast for D3 (white arrows in Figure 10a and Figure 11). Divide movements follow the inland position of a high-elevation, chevron-shaped plateau with elevations up to 170 m a.s.l. (Figures 2b and 10b). This plateau, not included in previous geomorphological maps of northeastern Brazil (e.g., Costa et al., 2020), developed over low-resistant Miocene and Quaternary deposits that overly resistant Precambrian basement rocks. The plateau configuration is sustained by incised tributaries, some showing headwaters close to each other (Figure 10b). An ongoing river capture between a tributary of the Paraíba River left bank and the upper Miriri River was recorded in the lower part of this plateau (white dot in Figure 10b).

5. Discussion

The present-day rivers of the Paraíba region show a set of features compatible with a transient landscape (Kirby and Whipple, 2012; Willett et al., 2014). Evidence includes non-linear χ-profiles bounded by knickpoints, bedrock river channels with spatially variable k_{sn}, and mobile drainage divide segments. These features were often recognized in erosional reliefs of tectonically active collisional mountain landscapes (Snyder et al., 2000; Wobus et al., 2006; Kirby and Whipple, 2012), rather than in the generally tectonically stable EPCMs (e.g., Gallen et al., 2013). The transient features recorded in the Precambrian highlands and coastal lowlands indicate that the Paraíba region had a topographic rejuvenation in the recent geological time due to fluvial disturbances. The significance of such transient features and the potential controlling factors that triggered the transient response in the late development of this passive continental margin are discussed below.

5.1. Dynamics and control on divide migration

The resulting χ-map and Gilbert metrics did not show many topographic or geometric changes in the fluvial channels and drainage divides of the studied seaward-dipping catchments. However, the migration of divides D2 and D3 (Figures 10 and 11) in the southeastern sector is due a lithological strength contrast. This is proposed because these divides occur in a plateau sustained by less resistant Miocene-Quaternary sedimentary units in contact with Precambrian basement rocks. However, the topographic expression of this plateau may not have formed primarily due to a lithological control. This plateau is topographically similar to the Shillong Plateau of northeast India (Strong et al., 2019). The Shillong Plateau resulted from the erosion of horizontally layered lithologies with contrasting resistances. This condition re-exposed a basement paleosurface, as proposed by numerical modelling of erosion (soft rocks over hard rocks; Forte et al., 2016). However, we interpret that the studied plateau was formed by a young tectonic uplift, i.e., probably due to the Late Pleistocene reactivation of the normal fault bounding the left margin of the Cariatá Graben (Bezerra et al., 2008), rather than the exhumation of bedrocks with contrasting erodibilities. This is evidenced by: i) the plateau covered by younger deposits (i.e., Late Quaternary Post-Barreiras Sediments) at higher elevations (i.e., up to 200 m a.s.l.) than adjacent Precambrian rocks (Figures 2b and 7); and ii) incised tributaries to the east of the plateau draining across a high-elevation Quaternary dome (Alves et al., 2019). Thus, the most likely is that tectonic uplift would have elevated basement rocks and overlying marine deposits, followed by fluvial incision and partial dissection of both the plateau and the dome.

Divide mobility to the southeast of the studied region is also supported by the current river capture between the left-bank tributary of the Paraíba River and the upper Miriri River (Figure 10). The headwater of the Paraíba River tributary at a lower base-level records accelerated headward erosion. This is evidenced by channel deepening and valley widening towards an elevated dome, where the Miriri River headwater is located. Once this fluvial connection has been completed, the less active Miriri River tributary will entrench south through the Paraíba Basin and abandon some of its uppermost stretches. Similar river capture has been recorded in other EPCMs, such as in the Ethiopian rift margin of northeast Africa (Giachetta and Willett, 2018). In the study area, the river capture will be of low magnitude and will result in the local re-organization of the drainage network.

5.2. Characterization of slope-break knickpoints

Slope-break knickpoints are presumed to propagate upstream at constant vertical rates, so they should occur at similar elevations (Neimann et al., 2001). This situation would be expected, for instance, in landscapes with invariant climatic, rock uplift and bedrock erodibility conditions, and where the drainage basins have similar geometric characteristics and incision dynamics. However, this expected transient response is generally rare in nature due to the variability of these factors and absence of an earlier steady-state that might disperse elevations during the knickpoint retreat (Boulton and Whittaker, 2009; Kirby and Whipple, 2012; Whipple et al., 2013). The range of knickpoint elevations (i.e., from 65 to 676 m a.s.l.) in the study area, especially in the Precambrian highlands (Figures 5, 6a and 7), and the weak statistical relationships including drainage area versus knickpoint elevation ($r^2 = 0.06$), and knickpoint elevation versus knickpoint distance from the mouth ($r^2 = 0.13$; Figure 9a-b), suggest either knickpoints with distinct formation or natural variability as a result of a single formation. Such conditions were documented in several other landscapes (e.g., Crosby and Whipple, 2006; Berlin and Anderson, 2007; Boulton and Whittaker, 2009; Boulton et al., 2014).

Basin gradient seems to explain, at least in part, the differences in statistical relationships (positive and negative) between the two knickpoint groups (southern and northern sectors) in the study area, which was higher for the southern basins. The differences of means between the two knickpoint groups only for the relative relief parameter (Table 3) indicated by the unpaired two-samples T-test, were expected given the high topographic heights of the graben from the southern sector. Alternatively, such differences in the relative relief are perhaps due to technical reasons, such as the configuration of the search window (e.g., Dibiase et al., 2010). The catchment dimensions might have been exceeded when larger radius thresholds were used (i.e., 3 and 5 km). The statistical similarities among most topographic parameters are perhaps indicative that the lowest knickpoints in each river are from a unique base-level fall. This event followed the Miocene, because some slope-break knickpoints were found on deposits of this age (Figures 2 and 6a). A previous simulations stated that fluvial disturbances are perceived generally in the order of 1–5 Myr time interval (Whittaker and Boulton, 2012). Thus, the fluvial disturbances in the study area occurred most likely in the Late Quaternary. This is also supported by tributaries incising into dome-like reliefs during this time. However, the migration of some knickpoints from most upstream catchment locations (e.g., rivers 5 and 6) is related to an earlier transient stage of the rivers.

The regression analysis pointing to the strong scalings ($r^2 > 0.89$) between the knickpoint horizontal distances and the drainage areas (Figure 9) suggests knickpoints not anchored in place. This observation is in line with records of horizontal knickpoint retreat as primarily a function of the drainage area (e.g., Crosby and Whipple, 2006; Berlin and Anderson, 2007; Boulton et al., 2014). The high variability of Hack's exponents by comparing the Cariatá Graben region (south) and the Patos Shear Zone region (north) is more likely due to the sinuosity of some large tributaries. Hence, the high sinuosity of the northern tributaries (e.g., rivers 5 and 6 in Figure 3) downstream of the knickpoints may have inflated part of the deviation of Hack's exponent ($L = 1.4A^{0.6}$;

Hack, 1957), as verified in other studies (Smart and Surkan, 1967; Willemin, 2000). However, the wide range of drainage areas upstream of knickpoints (i.e., from 2.4 to 238 km²) confirms that they are not pinned to a specific drainage area threshold, but are actively migrating upstream (Figure 9). The high scaling between the k_{sn} and the relative relief values (Figure 8b) further evidences that the tributaries are responding to a transient fluvial incision, with fluvial channels still adjusting to the new boundary conditions.

5.3. Control on knickpoints, k_{sn} variations, and fluvial incision

Transient features in fluvial landscapes, such as knickpoints and spatial variability in k_{sn} values, are indicative of base-level changes in response to boundary conditions. The knickpoint formation might be due to the exposure of rocks with differential erodibility, large river captures, and either spatial or temporal changes in past climate, sea-level and uplift rates (Wobus et al., 2006; Kirby and Whipple, 2012, Gallen, 2018). Our topographic analysis showed that some vertical-step knickpoints were lithologically controlled, as revealed by their: high scattering in the regression analysis (Figure 8b); absence of a clear spatial correspondence between some knickpoints and the structural fabric of the passive continental margin; and location close to lithological contacts of variable rock resistances (e.g., knickpoints from rivers 1 and 2 in Figure 6a and Supplementary Figure S4).Vertical-step knickpoints may reflect local contrasting lithologies, as shown in previous numerical modeling (e.g., Forte et al., 2016).

However, the high number of vertical-step knickpoints with significant increase in k_{sn} values downstream (Figure 8a) is a typical characteristic of slope-break knickpoints (Whipple et al., 2013). These knickpoints indicate the influence of a regional-scale factor. The uneven distribution of k_{sn} values (i.e., ranging from 8 to 462 $m^{0.9}$) in the highlands with Precambrian rocks to the west, where slope-break knickpoints follow a broad ~NNE-SSW- trend (see dashed blue lines in Figure 6a), is intriguing. Spatial variability of k_{sn} values in some EPCMs, such as in SE Brazil and eastern North America, was related to rock strength (Gallen, 2018; Peifer et al., 2021) or climatic control (Souza et al., 2019). However, in the highlands of the study area, the variability of k_{sn} values occurs across lithologies of relatively similar resistance (Figure 6a). In addition, climatic conditions, such as precipitation rates, do not vary significantly from the coast to the passive margin high relief zone (Carvalho et al., 2020). Thus, these factors could not have altered the channel dynamics, neither they could explain the regional k_{sn} variations in the study area.

Large river captures may alter the fluvial channel dynamics and produce knickpoints that propagate upstream (Whipple et al., 2017). However, the only ongoing river capture identified in the study area (Figure 10) is of a low magnitude, and it could not explain all knickpoints formed across the study area. The influence of eustatic sea-level lowering on knickpoints and k_{sn} variations is possible, particularly during the last glaciation maximum (ca. 23 and 18 ka), when the global sea-level reached 80-120 m below the modern sea level (e.g., Cutler et al., 2003; Clark et al., 2009). The extent to which the sea level controls inland base-level and fluvial incision is still uncertain, but 100-150 km upstream from the coast has generally been proposed (Blum and Törnqvist, 2000). The uppermost tributaries in the study area are located up to 125 km from the coast (Figure 8a), i.e., within the range of sea level influence. However, sea-level fall alone could not explain the increased fluvial incision (i.e., 156 m on average) in bedrock rivers on the Precambrian highlands (Table 2). In addition, a sustained base-level lowering longer than 100 ka is needed for the incision of tributary streams and migration of knickpoints (e.g., Whittaker and Boulton, 2012). Furthermore, the ~120 m global sea-level drop advocated for the Last Glaciation Maximum was fast, i.e., in the scale of orbital cycles of up to 100 ka (Cutler et al., 2003; Clark et al., 2009). Thus, its influence in the base-level changes and knickpoint propagation in this passive continental margin is unlikely.

We propose that the Late Quaternary tectonics controlled the formation of many knickpoints in the study area. Despite some differences in the proposed rates, several passive margins worldwide record increased rock uplift rates long after the rifting phase (Japsen et al., 2012; Pedoja et al., 2011; Gandini et al., 2014; Tribaldos et al., 2017), with multiple and regionalized uplift events during the Late Quaternary. For instance, a compilation of palaeoshoreline data (e.g., marine terraces) on a global scale with emphasis on the last interglacial stage (130-115 ka) showed that most coastal segments of passive margins were raised relative to sea-level due to an increase in the mean compression of the lithosphere (Pedoja et al., 2011). For the coastal segments to the north and south of the study area, they found an average uplift rate of only 0.1 mm/yr. However, a study integrating ichnological and sedimentary facies proposed a higher uplift rate of 0.63 mm/yr for the Paraíba region in the last 60 ka (Gandini et al., 2014). The rise of Late Pleistocene shallow marine deposits at ~38 m a.s.l reported by these authors is compatible with the fluvial incision averaging 43 m (Table 2) of some tributaries from the coastal lowlands of the study area. However, the low incision (140 m on average) of the rivers in this instance suggests a low-magnitude uplifting (Table 2), which resulted in limited topographic changes compared to those from tectonically active settings (Snyder et al., 2000; Wobus et al., 2006; Kirby and Whipple, 2012).

A trend of increased uplift rates in the last 30 Myr, with an increased peak since Middle Miocene (Figure 12), was recently documented for the Precambrian highlands

(Borborema Province) west of the study area, based on inverse modelling of river profiles (Tribaldos et al., 2017). In addition, the time scale for fluvial disturbances is generally lower than 5 Myr (Whittaker and Boulton, 2012). These data, together with the uplifting of Late Quaternary marine deposits in the Paraíba region (Gandini et al., 2014), led to relate the knickpoint migration and the knickpoints at higher elevations in the Precambrian highlands (Table 2 and Figures 8a) to variations in Late Quaternary uplift rates. The displacement of recent alluvial deposits with offsets up to 100 m following the main drainage courses in the Cariatá Graben region (Fonsêca et al., 2020) is consistent with uplifting timing.

Figure 12.

The differential erosion of the studied relief is probably due to large rivers that drained the Precambrian terrains, as these rivers have higher potential of erosion than the smaller and less erosive rivers from the coastal lowlands to the east. However, extensive fracturing during and after the pre-rift stage could have enhanced the likelihood of erosion in the low-lying Precambrian rocks to the west. A numerical modelling of reliefs traversed by shear zones compared to the studied Precambrian terrains has indicated that fluvial incision rates close to areas with joints, fractures and faults are orders of magnitude faster than in adjacent intact bedrocks (Roy et al., 2015). In the instance of the study area, many tributary streams are (Figure 3) aligned according to regional E-W, NE-SW and NW-SE structural trends (Bezerra et al., 2011). For instance, the Cariatá Graben subsided due to the reactivation of normal faults during the Late Quaternary (Bezerra et al., 2008). In addition, the reactivation of normal faults and major dextral strike-slip mylonitic belts are recorded along the Patos and Pernambuco shear zones due to transpressional/transtensional deformation (Bezerra et al., 2014, 2020; Nogueira et al., 2015). These pre-existing structures were reactivated several times during the post-rift development of the northeastern Brazilian passive continental margin, with the youngest reactivation occurring in the Quaternary (e.g., Bezerra et al., 2008; Marques et al., 2014; Nogueira et al., 2015). Tectonic reactivation along the Patos Shear Zone raised the Araripe Plateau (Marques et al., 2014) and Rio do Peixe Basin (Nogueira et al., 2015), located to the west of the study area, in tens of meters. In addition, the Pernambuco Shear Zone is a present-day well-known active seismogenic zone that concentrate a high number of low to moderate magnitude earthquakes (e.g., Lima Neto et al., 2013; Figure 1). Thus, we propose that the study area was uplifted due to the reactivation of pre-existing structural trends. The tectonic reactivation is likely to have triggered the incision wave that migrated upstream into the drainage systems to produce the mobile knickpoints and incised river channels in the highlands. This interpretation agrees with the fact that the knickpoints lie upstream of the Patos Shear Zone to the north and upstream of normal faults of the Cariatá Graben to the south (Figure 7).

5.4. Mechanisms for the passive margin uplift in the Paraíba region

There is no general agreement on the mechanisms that cause regional uplifting of passive continental margins. Main hypotheses are mantle forcing (Cox, 1989) and increased lithosphere compression due to plate interactions (Leroy et al., 2004). The latter produces stresses with far-field effects even thousands of kilometres far from the stress source (e.g., at plate boundaries). Stresses produced at the plate boundaries are transmitted across the lithosphere and are accommodated by pre-existing weakness zones of the crust, such as shear zones. These zones are eventually reactivated to produce differential uplifts (Holdsworth et al., 1997). Several works have demonstrated that far-field stresses can be responsible for intraplate faulting and seismicity in passive margins and intracontinental settings (Zoback, 1992; Assumpção and Araújo, 1993; Hill et al., 1995; Pedoja et al., 2011; Japsen et al., 2012). For instance, the rise of the Andean mountain range and the continuous lateral growth of the Andean Plateau caused a local compression that increased the regional compression of the entire South American platform (Assumpção and Araújo, 1993). Similarly, the long distance (i.e., 3500 km) transmission of compressional stresses through the lithosphere caused basin inversions in southeast Australia (Hill et al., 1995).

Intraplate compression due to motions of the Mid-Atlantic Ridge (MAR) pushing towards the west, and of the Andean Chain pushing towards the east, was interpreted as the main mechanism for post-rift tectonic reactivation and inversion of many sedimentary basins in the northeastern Brazilian passive continental margin (Marques et al., 2014; Nogueira et al., 2015; Vasconcelos et al., 2019; Bezerra et al., 2020). These studies proposed that tectonic inversion of the sedimentary basins in this passive margin would have occurred during three main phases of Andean tectonism: Peruvian (80-65 Myr), Incaic (45-28 Myr), and Quechuan (22-0 Myr; Coutand et al., 2001; Garzione et al., 2008). Whilst the oldest compressional event is difficult to describe due to the long-term erosion (Marques et al., 2014), the record of normal/reverse faults and folds in Miocene and Late Quaternary deposits in this margin (Rossetti et al., 2011a, 2011b; Bezerra et al., 2014; Alves et al., 2019; Andrades Filho et al., 2021) agrees with the influence of the Quechuan compressional event. Post-rift (Miocene and Quaternary) tectonic deformation, including both extension and compression, is compatible with the present-day stress-field documented in northeastern Brazil, that is, E-W compression and N-S oriented extension within a strike-slip deformational regime (Bezerra et al., 2014).

The timing of knickpoint formation in the Paraíba region, presumably of Late Quaternary age, matches with the Quechuan tectonic phase, which occurred when the

Andean Plateau was exceptionally high (Garzione et al., 2008; see paleoelevations in Figure 12). The synchronicity between this compressional event and the fluvial disturbances observed in the study area suggests a causative link between far-field stress-induced tectonic uplifting and base-level lowering.

6. Conclusion

DEM-based river profile and divide migration analyses helped to decode the post-rift geomorphic history of the South American EPCM in the Paraíba region. These methods have the potential to inform short-term events in the evolution of EPCMs, particularly in regions with limited or lack of field-based geological data. The results of the topographic analysis showed that the overall drainage routing pattern of the Paraíba region is sustained by the broad configuration of the passive continental margin, with a highland plateau composed of pre-rift bedrocks of varied strengths and tectonic fabrics. In contrast to proposals of stable passive margins over the last million years, this study shows that the late development of the studied EPCM was marked by increased local tectonics during the Late Quaternary. This event changed the topographic gradient and likely accelerated the erosion, as informed by a number of transient fluvial features, such as: mobile knickpoints; incised fluvial channels with increased k_{sn}; and divide migration, many of which recorded over lithologies with similar resistances at or close to the uplifted zones. Spatial variations in the uplift rates, potentially driven by far-field compressive stresses concentrated in the shear zones, resulted in base-level lowering, headward erosion, and drainage divide upstream migration, with drainage reorganizations taking place along the drainage divides. These results support previous studies that the topographic development and final stages of evolution of the eastern South America passive continental margin had a tectonic contribution, at least in its northeastern sector.

Acknowledgements

This study was financed by the Coordination for the Improvement of Higher Education Personnel - Institutional Program for Internationalization (CAPES-PRINT) within the Satellite Applications for Sustainable Development project from the National Institute for Space Research – INPE in Brazil. The School of Geography, Earth and Environmental Sciences of the University of Plymouth is acknowledged for providing the workstation for data processing. We would like to thank Jesse R. Zondervan for helping the rock strength and divide migration analyses and for the scientific discussions, which helped to improve an earlier version of this work. Authors are scholarship holders of the Council for Scientific and Technological Development (CNPq), processes 307943/2019-4 (M.M.V.), 163159/2020-3 (F.C.A.) and 301343/2018-7 (D.F.R.). Finally, we thank the two anonymous reviewers and the editor, Achim Beylich, for comments that improved this article.

References

Almeida, F.F.M., Hasui, Y., Brito Neves, B.B., Fuck, R.A., 1981. Brazilian structural provinces: An introduction. Earth-Science Reviews. 17, 1–29. https://doi.org/10.1016/0012-8252(81)90003-9

Alves, F.C., Rossetti, D.F., Valeriano, M.M., Andrades Filho, C.O., 2019. Neotectonics in the South American passive margin: Evidence of Late Quaternary uplifting in the northern Paraiba Basin (NE Brazil). Geomorphology. 325, 1-16. https://doi.org/10.1016/j.geomorph.2018.09.028

Andrades Filho, C.O., Rossetti, D.F., Bezerra, F.H.R., 2021. The unsteady post-rift stage of the South American passive margin based on the tectono-sedimentary evolution of the onshore Paraíba Basin, NE Brazil. Quaternary International. https://doi.org/10.1016/j.quaint.2020.10.051

Assumpção, M., Araújo, M., 1993. Effect of the Altiplano-Puna plateau, South America, on the regional intraplate stresses. Tectonophysics. 221, 475-496. https://doi.org/10.1016/0040-1951(93)90174-I

Barbosa, J.A., Souza, E., Lima Filho, M., Neumann, V.A., 2003. Estratigrafia da Bacia Paraíba: uma reconsideração. Estud. Geol. 13, 89–108.

Berlin, M.M., Anderson, R.S., 2007. Modeling of knickpoint retreat on the Roan Plateau, western Colorado. Journal of Geophysical Research: Earth Surface. 112, 1–16. https://doi.org/10.1029/2006JF000553

Bernard, T., Sinclair, H.D., Gailleton, B., Mudd, S.M., Ford, M., 2019. Lithological control on the post-orogenic topography and erosion history of the Pyrenees. Earth and Planetary Science Letters. 518, 53–66. https://doi.org/10.1016/j.epsl.2019.04.034

Bezerra, F.H., Vita-Finzi, C., 2000. How active is a passive margin? Palaeoseismicity in Northeastern Brazil. Geology. 28, 591–594. https://doi.org/10.1130/0091-7613(2000)28%3C591:HAIAPM%3E2.0.CO;2

Bezerra, F.H., Brito Neves, B.B., Corrêa, A.C., Barreto, A.M., Suguio, K., 2008. Late Pleistocene tectonic-geomorphological development within a passive margin - The Cariatá trough, northeastern Brazil. Geomorphology. 97, 555–582. https://doi.org/10.1016/j.geomorph.2007.09.008

Bezerra, F.H., Nascimento, A.F., Ferreira, J.M., Nogueira, F.C., Fuck, R.A., Neves, B.B., Sousa, M.O., 2011. Review of active faults in the Borborema Province, Intraplate South America - Integration of seismological and paleoseismological data. Tectonophysics. 510, 269–290. https://doi.org/10.1016/j.tecto.2011.08.005

Bezerra, F.H., Rossetti, D.F., Oliveira, R.G., Medeiros, W.E., Neves, B.B., Balsamo, F., Nogueira, F.C., Dantas, E.L., Andrades Filho, C.O., Góes, A.M., 2014. Neotectonic reactivation of shear zones and implications for faulting style and geometry in the continental margin of NE Brazil. Tectonophysics. 614, 78–90. https://doi.org/10.1016/j.tecto.2013.12.021

Bezerra, F.H., Castro, D.L., Maia, R.P., Sousa, M.O., Moura-Lima, E.N., Rossetti, D.F., Bertotti, G., Souza, Z.S., Nogueira, F.C., 2020. Postrift stress field inversion in the Potiguar Basin, Brazil – Implications for petroleum systems and evolution of the equatorial margin of South America. Marine and Petroleum Geology.111, 88–104. https://doi.org/10.1016/j.marpetgeo.2019.08.001

Bianchi, M.B., M. Assumpção, M.P., Rocha, J.M., Carvalho, P.A., Azevedo, S.L., Fontes, F.L., Dias, J.M., Ferreira, A.F., Nascimento, M.V., Ferreira, Costa, I.S.L., 2018. The Brazilian Seismographic Network (RSBR): Improving Seismic Monitoring in Brazil. Seism. Res. Lett. 89, 452-457. doi: 10.1785/0220170227

Bierman, P.R., Caffee, M., 2001. Slow rates of rock surface erosion and sediment production across the Namib desert and escarpment, Southern Africa. American Journal of Science. 301, 326-358. https://doi.org/10.2475/ajs.301.4-5.326

Blum, M.D., Törnqvist, T.E., 2000. Fluvial responses to climate and sea-level change: a review and look forward. Sedimentology. 47, 2-48. https://doi.org/10.1046/j.1365-3091.2000.00008.x

Boulton, S.J., Whittaker, A.C., 2009. Quantifying the slip rates, spatial distribution and evolution of active normal faults from geomorphic analysis: field examples from an oblique-extensional graben, southern Turkey. Geomorphology. 104, 299–316. https://doi.org/10.1016/j.geomorph.2008.09.007

Boulton, S.J., Stokes, M., Mather, A.E., 2014. Transient fluvial incision as an indicator of active faulting and Plio-Quaternary uplift of the Moroccan high Atlas. Tectonophysics. 633, 16–33. https://doi.org/10.1016/j.tecto.2014.06.032

Boulton, S.J., Stokes, M., 2018. Which DEM is best for analyzing fluvial landscape development in mountainous terrains?. Geomorphology. 310, 168-187. https://doi.org/10.1016/j.geomorph.2018.03.002

Bradley, D.C., 2008. Passive margins through earth history. Earth-Science Reviews. 91,1-26. https://doi.org/10.1016/j.earscirev.2008.08.001

Brito Neves, B.B., Riccomini, C., Fernandes, T.M.G., Santanna, L.G., 2004. O sistema tafrogênico terciário do saliente oriental nordestino na Paraíba: um legado Proterozóico. Revista Brasileira de Geociências. 1, 127–134.

Bursztyn, N., Pederson, J.L., Tressler, C., Mackley, R.D., Mitchell, K.J., 2015. Rock strength along a fluvial transect of the Colorado Plateau - quantifying a fundamental control on geomorphology. Earth and Planetary Science Letters. 429, 90–100. https://doi.org/10.1016/j.epsl.2015.07.042

Carvalho, A.A., Montenegro, A.A.A., Silva, H.P., Lopes, I., Morais, J.E.F., Silva, T.G.F., 2020. Trends of rainfall and temperature in Northeast Brazil. Revista Brasileira de Engenharia Agrícola e Ambiental. 24, 15–23. https://doi.org/10.1590/1807-1929/agriambi.v24n1p15-23

Clark, P.U., Dyke, A.S., Shakun, J.D., Carlson, A.E., Clark, J.,Wohlfarth, B., Mitrovica, J.X., Hostetler, S.W., McCABE, M., 2009. The last glacial maximum. Science. 325, 710–714. https://doi.org/10.1126/science.1172873

Cobbold, P.R., Meisling, K.E., Mount, V.S., 2001. Reactivation of an obliquely rifted margin, Campos and Santos basins, southeastern Brazil. AAPG Bulletin. 85, 1925-1944. https://doi.org/10.1306/8626D0B3-173B-11D7-8645000102C1865D

Costa, L.R.F., Maia, R.P., Barreto, L.L., Sales, V.C.C., 2020. Geomorfologia do nordeste setentrional brasileiro: uma proposta de classificação. Revista Brasileira de Geomorfologia. 21, 185-208. http://dx.doi.org/10.20502/rbg.v21i1.1447

Coutand, I., Cobbold, P.R., Urreiztieta, M., Gautier, P., Chauvin, A., Gapais, D., Rossello, E.A., López-Gamundí, O., 2001. Style and history of Andean deformation, Puna plateau, northwestern Argentina. Tectonics. 20, 210–234. https://doi.org/10.1029/2000TC900031

Cox, K.G., 1989. The role of mantle plumes in the development of continental drainage patterns. Nature. 342, 873–877.

Crosby, B.T., Whipple, K.X., 2006. Knickpoint initiation and distribution within fluvial networks: 236 waterfalls in the Waipaoa River, North Island, New Zealand. Geomorphology. 82, 16–38. https://doi.org/10.1016/j.geomorph.2005.08.023

Cutler, K.B., Edwards, R.L., Taylor, F.W., Cheng, H., Adkins, J., Gallup, C.D., Cutler, P.M., Burr, G.S., Bloom, A.L., 2003. Rapid sea-level fall and deep-ocean temperature change since the last interglacial period. Earth and Planetary Science Letters. 206, 253–271. https://doi.org/10.1016/S0012-821X(02)01107-X

DiBiase, R.A., Whipple, K.X., Heimsath, A.M., Ouimet, W.B., 2010. Landscape form and millennial erosion rates in the San Gabriel Mountains, CA. Earth and Planetary Science Letters. 289, 134–144. https://doi.org/10.1016/j.epsl.2009.10.036

Farr, T.G., Rosen, P.A., Caro, E., Crippen, R., Duren, R., Hensley, S., Kobrick, M., Paller, M., Rodriguez, E., Roth, L., Seal, D., Shaffer, S., Shimada, J., Umland, J., Werner, M., Oskin, M., Burbank, D., Alsdorf, D., 2007. The Shuttle radar topography mission. Rev. Geophys. 45, 1–33. https://doi.org/10.1029/2005RG000183

Fonsêca, D.N., Corrêa, A.C.B., Tavares, B.A.C., Lira, D.R., Barros, A.C.M., Mutzenberg, D.S., 2020. Coupling of tectonic factors and precipitation variability as a driver of Late Quaternary aggradation in Northeast Brazil. Earth Surface Processes and Landforms. 45, 3525-3539.

Forte, A.M., Yanites, B.J., Whipple, K.X., 2016. Complexities of landscape evolution during incision through layered stratigraphy with contrasts in rock strength. Earth Surface Processes and Landforms. 41, 1736–1757. https://doi.org/10.1002/esp.3947

Forte, A.M., Whipple, K.X., 2018. Criteria and tools for determining drainage divide stability. Earth and Planetary Science Letters. 493, 102–117. https://doi.org/10.1016/j.epsl.2018.04.026

Forte, A.M., Whipple, K.X., 2019. Short communication: The Topographic Analysis Kit (TAK) for TopoToolbox. Earth Surface Dynamics. 7, 87–95. https://doi.org/10.5194/esurf-7-87-2019

Gallagher, K., Brown, R., Johnson, C., 1998. Fission track analysis and its applications to geological problems. Annual Review of Earth and Planetary Sciences. 26, 519–572. https://doi.org/10.1146/annurev.earth.26.1.519

Gallen, S.F., Wegmann, K.W., Bohnenstiehl, D.W.R., 2013. Miocene rejuvenation of topographic relief in the southern Appalachians. GSA Today. 23, 4–10. 10.1130/GSATG163A.1

Gallen, S.F., Wegmann, K.W., 2017. River profile response to normal fault growth and linkage: An example from the Hellenic forearc of south-central Crete, Greece. Earth Surface Dynamics. 5, 161–186. https://doi.org/10.5194/esurf-5-161-2017

Gallen, S.F., 2018. Lithologic controls on landscape dynamics and aquatic species evolution in post-orogenic mountains. Earth and Planetary Science Letters. 493, 150–160. https://doi.org/10.1016/j.epsl.2018.04.029

Gandini, R., Rossetti, D.F., Netto, R.G., Bezerra, F.H.R., Góes, A.M., 2014. Neotectonic evolution of the Brazilian northeastern continental margin based on sedimentary facies and ichnology. Quaternary Research (United States). 82, 462–472. https://doi.org/10.1016/j.yqres.2014.07.003

Garzione, C.N., Hoke, G.D., Libarkin, J.C., Withers, S., Macfadden, B., Eiler, J., Ghosh, P., Mulch, A., 2008. Rise of the Andes. Science. 320, 1304-1307. https://doi.org/10.1126/science.1148615

Giachetta, E., Willett, S.D., 2018. Effects of River Capture and Sediment Flux on the Evolution of Plateaus: Insights From Numerical Modeling and River Profile Analysis in the Upper Blue Nile Catchment. Journal of Geophysical Research: Earth Surface. 123, 1187-1217. https://doi.org/10.1029/2017JF004252

Gilchrist, A.R., Summerfield, M.A., 1990. Differential denudation and flexural isostasy in formation of rifted-margin upwarps. Nature. 346, 739-742.

Gómez, J., Schobbenhaus, C. & Montes, N.E., compilers. 2019. Geological Map of South America 2019. Scale 1:5 000 000. Commission for the Geological Map of the World (CGMW), Colombian Geological Survey and Geological Survey of Brazil. Paris.

Goren, L., Willett, S.D., Herman, F., Braun, J., 2014. Coupled numerical–analytical approach to landscape evolution modeling. Earth Surface Processes and Landforms. 39, 522-545. https://doi.org/10.1002/esp.3514

Goudie, A.S., 2006. The Schmidt Hammer in geomorphological research. Progress in Physical Geography. 30, 703-718. https://doi.org/10.1177%2F0309133306071954

Hack, J.T., 1957. Studies of Longitudinal Stream Profiles in Virginia and Maryland. U.S.G.S. Professional Paper 294-B, pp. 1–91.

Haviv, I., Enzel, Y., Whipple, K. X., Zilberman, E., Matmon, A., Stone, J., and Fifield, K. L. 2010. Evolution of vertical knickpoints (waterfalls) with resistant caprock: Insights from numerical modeling, J. Geophys. Res., 115, F03028. https://doi.org/10.1029/2008JF001187

He, C., Rao, G., Yang, R., Hu, J., Yao, Q., Yang, C.J., 2019. Divide migration in response to asymmetric uplift: Insights from the Wula Shan horst, North China. Geomorphology. 339, 44-57. https://doi.org/10.1016/j.geomorph.2019.04.024

Henderson, F.M., Lewis, A.J., 1998. Principles and Applications of Imaging Radar: Manual of remote sensing. New York: John Wiley and Sons.

Hill, K.C., Hill, K A., Cooper, G.T., O'Sullivan, A.J., O'sullivan, P.B., Richardson, M.J., 1995. Inversion around the Bass Basin, SE Australia. In J. G. Buchanan, & P. G. Buchanan (Eds.), Basin Inversion. Geological Society, London, Special Publications 88, 525–547.

Holdsworth, R.E., Butler, C.A., Roberts, A.M., 1997. The recognition of reactivation during continental deformation. Journal of the Geological Society, London. 154, 73–78.

Japsen, P., Chalmers, J.A., Green, P.F., Bonow, J.M., 2012. Elevated, passive continental margins: Not rift shoulders, but expressions of episodic, post-rift burial and exhumation. Global and Planetary Change. 90-91, 73–86. https://doi.org/10.1016/j.gloplacha.2011.05.004

King, L.C., 1967. The Morphology of the Earth. Oliver and Boyd, Edinburgh.

Kirby, E., Whipple, K.X., 2012. Expression of active tectonics in erosional landscapes. Journal of Structural Geology. 44, 54–75. https://doi.org/10.1016/j.jsg.2012.07.009

Lague, D., 2014. The stream power river incision model: evidence, theory and beyond. Earth Surface Processes and Landforms. 39, 38–61. https://doi.org/10.1002/esp.3462

Leroy, M., Dauteuil, O., Cobbold, P.R., 2004. Incipient shortening of a passive margin: The mechanical roles of continental and oceanic lithospheres. Geophysical Journal International. 159, 400–411. https://doi.org/10.1111/j.1365-246X.2004.02400.x

Lima Neto, H.C., Ferreira, J.M., Bezerra, F.H.R., Assumpção,M.S., Do Nascimento, A.F., Sousa, M.O.L.,Menezes, E.A.S., 2013. Upper crustal earthquake swarms in São Caetano: reactivation of the Pernambuco shear zone and trending branches in intraplate Brazil. Tectonophysics 608, 804–811. https://doi.org/10.1016/j.tecto.2013.08.001

Marques, F.O., Nogueira, F.C., Bezerra, F.H., Castro, D.L., 2014. The Araripe Basin in NE Brazil: An intracontinental graben inverted to a high-standing horst. Tectonophysics. 630, 251–264. https://doi.org/10.1016/j.tecto.2014.05.029

Matos, R.M.D., 1992. The Northeast Brazilian Rift System. Tectonics. 11, 766–791.

Morais Neto, J.M., Green, P.F., Karner, G.D., Alkmim, F.F., 2008. Age of the Serra do Martins Formation, Borborema Plateau, northeastern Brazil: constraints from apatite and zircon fission track analysis. Bol. Geoc. Petrobras 16, 23–52.

Neimann, J.D., Gasparini, N.M., Tucker, G.E., Bras, R.L., 2001. A quantitative evaluation of Playfair's law and its use in testing long-term stream erosion models. Earth Surface Processes and Landforms. 26, 1317–1332.

Noether, G.E., 1991. Introduction to Statistics: The Nonparametric Way. Stanford, CA: Springer Science Business Media, LLC.

Nogueira, F.C., Marques, F.O., Bezerra, F.H., Castro, D.L., Fuck, R.A., 2015. Cretaceous intracontinental rifting and post-rift inversion in NE Brazil: Insights from the Rio do Peixe Basin. Tectonophysics. 644, 92–107. https://doi.org/10.1016/j.tecto.2014.12.016

Ollier, C.D., Pain, C.F., 1997. Equating the basal unconformity with the palaeoplain: a model for passive margins. Geomorphology. 19, 1-15.

Pedoja, K., Husson, L., Regard, V., Cobbold, P.R., Ostanciaux, E., Johnson, M.E., Kershaw, S., Saillard, M., Martinod, J., Furgerot, L., Weill, P., Delcaillau, B., 2011.

Relative sea-level fall since the last interglacial stage: Are coasts uplifting worldwide? Earth-Science Reviews. 108, 1–15. https://doi.org/10.1016/j.earscirev.2011.05.002

Peifer, D., Persano, C., Hurst, M.D., Bishop, P., Fabel, D., 2021. Growing topography due to contrasting rock types in a tectonically dead landscape. Earth Surf. Dyn. 9, 167–181. https://doi.org/10.5194/esurf-9-167-2021

Perron, J.T., Royden, L., 2013. An integral approach to bedrock river profile analysis. Earth Surface Processes and Landforms. 38, 570–576. https://doi.org/10.1002/esp.3302

Roy, S.G., Koons, P.O., Upton, P., Tucker, G.E., 2015. The influence of crustal strength fields on the patterns and rates of fluvial incision. J. Geophys. Res. Earth Surf., 120: 275– 299. https://doi.org/10.1002/2014JF003281

Rossetti, D.F., Bezerra, F.H.R., Góes, A.M., Valeriano, M.M., Andrades Filho, C.O., Mittani, J.C.R., Tatumi, S.H., Brito Neves, B.B., 2011a. Late Quaternary sedimentation in the Paraíba Basin, Northeastern Brazil: Landform, sea level and tectonics in Eastern South America passive margin. Palaeogeography, Palaeoclimatology, Palaeoecology. 300, 191–204. https://doi.org/10.1016/j.palaeo.2010.12.026

Rossetti, D.F., Bezerra, F.H.R., Góes, A.M., Neves, B.B.B., 2011b. Sediment deformation in Miocene and post-Miocene strata, Northeastern Brazil: Evidence for paleoseismicity in a passive margin. Sedimentary Geology. 235, 172–187. https://doi.org/10.1016/j.sedgeo.2010.02.005

Rossetti, D.F., Góes, A.M., Bezerra, F.H., Valeriano, M.M., Brito Neves, B.B., Ochoa, F.L., 2012. Contribution to the stratigraphy of the onshore Paraíba basin, Brazil. Anais da Academia Brasileira de Ciencias. 84, 313–333. https://doi.org/10.1590/S0001-37652012005000026

Rossetti, D.F., Bezerra, F.H., Dominguez, J.M.L., 2013. Late Oligocene-Miocene transgressions along the equatorial and eastern margins of Brazil. Earth-Sci. Rev. 123, 87–112. https://doi.org/10.1016/j.earscirev.2013.04.005.

Schwanghart, W., Scherler, D., 2014. Short Communication: TopoToolbox 2 - MATLAB-based software for topographic analysis and modeling in Earth surface sciences. Earth Surface Dynamics. 2, 1–7. https://doi.org/10.5194/esurf-2-1-2014.

Smart, J.S., Surkan, A.J., 1967. The relation between mainstream length and area in drainage basins. Water Resources Research. 3, 963–974.

Snyder, N.P., Whipple, K.X., Tucker, G.E., Merritts, D.J., 2000. Stream profiles in the Mendocino triple junction region, northern California. GSA Bulletin. 112, 1250-1263.

Strahler, A.N., 1957. Quantitative analysis of watershed geomorphology. Trans. Am. Geophys. Union 38, 913–920

Strong, C. M., Attal, M., Mudd, S.M., Sinclair, H.D., 2019. Lithological control on the geomorphic evolution of the Shillong Plateau in Northeast India. Geomorphology. 330, 133–150. https://doi.org/10.1016/j.geomorph.2019.01.016

Souza, D. H., Stuart, F.M., Rodés, A., Pupim, F.N., Hackspacher, P.C., 2019. Controls on the erosion of the continental margin of southeast Brazil fromcosmogenic10Be in river sediments. Geomorphology. 330: 163-176. https://doi.org/10.1016/j.geomorph.2019.01.020

Tribaldos, R.V., White, N.J., Roberts, G.G., Hoggard, M.J., 2017. Spatial and temporal uplift history of South America from calibrated drainage analysis. Geochemistry, Geophysics, Geosystems. 18, 2321–2353. https://doi.org/10.1002/2017GC006909

Vasconcelos, D.L., Bezerra, F.H., Medeiros, W.E., Castro, D.L., Clausen, O.R., Vital, H., Oliveira, R.G., 2019. Basement fabric controls rift nucleation and postrift basin inversion in the continental margin of NE Brazil. Tectonophysics. 751, 23–40. https://doi.org/10.1016/j.tecto.2018.12.019

Venables WN, Smith DM. 2002. An Introduction to R. Network Theory, Bristol, UK

Whipple, K.X., DiBiase, R., Crosby, B., 2013. Bedrock rivers. In: Shroder, J. (Ed.), Treatise on Geomorphology, vol. 9. Academic Press, San Diego, CA, pp. 550–573.

Whipple, K.X., Forte, A.M., Dibiase, R.A., Gasparini, N.M., Ouimet, W.B., 2017. Timescales of landscape response to divide migration and drainage capture: Implications for the role of divide mobility in landscape evolution. Journal of Geophysical Research: Earth Surface. 122, 248–273. https://doi.org/10.1002/2016JF003973

Whittaker, A.C., Boulton, S.J., 2012. Tectonic and climatic controls on knickpoint retreat rates and landscape response times. Journal of Geophysical Research: Earth Surface. 117, 1–19. https://doi.org/10.1029/2011JF002157

Willemin, J.H., 2000. Hack's law: Sinuosity, convexity, elongation. Water Resources Research. 36, 3365–3374. https://doi.org/10.1029/2000WR900229

Willett, S.D., Mccoy, S.W., Taylor Perron, J., Goren, L., Chen, C.Y., 2014. Dynamic reorganization of River Basins. Science. 343, 1–19. https://doi.org/10.1126/science.1248765

Wobus, C., Whipple, K.X., Kirby, E., Snyder, N., Johnson, J., Spyropolou, K., Crosby, B., Sheehan, D., 2006. Tectonics from topography: Procedures, promise, and pitfalls. Special Paper of the Geological Society of America. 398, 55–74. https://doi.org/10.1130/2006.2398(04)

Zondervan, J.R., Stokes, M., Boulton, S.J., Telfer, M.W., Mather, A.E., 2020. Rock strength and structural controls on fluvial erodibility: Implications for drainage divide mobility in a collisional mountain belt. Earth and Planetary Science Letters. 538, 116221. https://doi.org/10.1016/j.epsl.2020.116221

Zoback, M. L., 1992. First- and second-order patterns of stress in the lithosphere: The World Stress Map Project. J. Geophys. Res. 97, 11703. https://doi.org/10.1029/92JB00132

Figure Captions

Figure 1. Continental scale geological framework and epicentral distribution in the northeastern Brazilian passive continental margin. Shear zones: Pa = Patos; Pe = Pernambuco. Sedimentary basins: Ar = Araripe; Ig = Iguatú; Ja = Jatobá; Po = Potiguar; Pn = Parnaíba; RP = Rio do Peixe; SA = Sergipe-Alagoas; Tu = Tucano; Pe = Pernambuco; and Pb = Paraíba. Geological compartments and structures modified from the Brazilian Geological Survey (CPRM) database (http://geosgb.cprm.gov.br/geosgb) and the geological map of South America at 1:5.000.000 scale (Gómez et al., 2019). Instrumental earthquake data (white circles) available for the period of 1955 to 2020 was simplified from the Brazilian Seismic Catalog (Bianchi et al., 2018; http://moho.iag.usp.br/eq/bulletin/).

Figure 2. Geological context and regional topography of the study area. (a) Geology of the passive continental margin and location of main trunk streams. Trunk rivers: Cu = Curimataú; Ca = Camaratuba; Ma = Mamanguape; Mi = Miriri; Pb = Paraíba. Shaded relief derived from the SRTM-DEM. Geological units simplified from the CPRM geological map at 1:1000000 scale (http://geosgb.cprm.gov.br/geosgb). (b) Swath topographic profile derived from the SRTM-DEM, with the regional morphology of the passive continental margin.

Figure 3. Location of the tributary streams investigated in the study area and major tectonic structures. Pa-sz = Patos shear zone. Trunk streams: Cu = Curimataú; Ca = Camaratuba; Ma = Mamanguape; Mi = Miriri; and Pb =Paraíba River. Dashed black line = inferred fault in the basin. RDD = Regional drainage divide. Geological classes simplified from the geological map at 1:1000000 scale from CPRM

(http://geosgb.cprm.gov.br/geosgb). The location of the shear zone and graben-related normal faults based on Bezerra et al. (2008, 2014).

Figure 4. River profiles of tributary streams from the study area without apparent knickpoints (see location of numbered tributaries in Figure 3). (a-c) River profiles in distance-elevation plots. (d-f) River profiles in χ-elevation plots. Trunk streams with knickpoints are also indicated for comparison. Trunk streams: Cu = Curimataú; Ma = Mamanguape; Pb = Paraiba. River profiles were coloured by their corresponding geology. River profile segments related to artifacts (lakes/reservoirs) are shown only in the distance-elevation graphs for the sake of simplification.

Figure 5. River profiles of tributary streams from the study area showing knickpoints (slope-break and vertical-step). (a-c) River profiles in distance-elevation plots. (d-f) River profiles in χ-elevation plots (see the location of numbered tributaries in Figure 3). Trunk streams: Cu = Curimataú; Ma = Mamanguape; Pb = Paraíba. River profile segments related to artifacts (lakes/reservoirs) shown only in distance-elevation plots for simplification. River profiles coloured by their corresponding geology. (g-h-i) Log-log slope-area (black dots) and χ-elevation plots with examples of profiles bounded by vertical-step (g), slope-break (h), and both (i). A_{cr} = critical drainage area.

Figure 6. K_{sn} spatial distribution and rock strength analysis. (a) Drainage network coloured by k_{sn} values, with the location of knickpoints, drainage basins, and spatial contacts of rock groups of similar relative resistance to erosion (see Table 1 for definition of rock groups). K_{sn} values were classified by quantiles due to their skewed distribution. Major trunk streams: Cu = Curimataú; Ca = Camaratuba; Ma = Mamanguape; Mi = Miriri; Pb = Paraíba. RDD = Regional drainage divide. Dashed blue line = inferred area of high relief. (b) Average k_{sn} and standard deviation values for

each rock group (Sr = sedimentary rocks; Mr = metamorphic rocks; and Imr = igneous and meta-igneous rocks). The number of samples is displayed besides each error bar.

Figure 7. 3D-view of the EPCM based on the SRTM-DEM (vertical exaggeration of 30×), with the location of tributaries, slope-break knickpoints and main tectonic structures. Purple dot = slope-break knickpoint (numbered tributaries); blue line = tributary streams. HEP = High-elevation plateau; LRS = Low-relief surface; HECP = high-elevation, chevron-shaped plateau; DR = dome-like relief; CP = coastal plain. Solid black line = normal fault; dashed black line = dextral strike-slip fault. Dashed white line = general limits between basement rocks to the west and sedimentary covers to the east. The location of the Patos shear zone and faults bounding the Cariatá Graben was based on Bezerra et al. (2008, 2014).

Figure 8. Statistic analysis of knickpoints from the study area. (a) Distribution of average k_{sn} values upstream and downstream of knickpoints and knickpoint elevations from the coastline (E-W). (b) Linear regression between k_{sn} at knickpoint (slope-break and vertical-step) and relative relief.

Figure 9. Statistic analysis of the slope-break knickpoints. Linear regressions: (a) drainage area versus knickpoint elevation; (b) knickpoint elevation versus knickpoint distance from the mouth; (c) total drainage area versus knickpoint distance from the mouth; (d) drainage area above knickpoint versus knickpoint distance from the divide; and (e) drainage area below knickpoint versus knickpoint distance from the mouth. The distributions in c-d-e were fitted by a power-law function in the general form of Hack's law ($L = kA^h$; Hack, 1957).

Figure 10. χ-map for the complete drainage basins of the passive continental margin (outlets ≥ 1m asl) and the 3D-view of an ongoing river capture. Trunk streams in a: Cu

= Curimataú; Ca = Camaratuba; Ma = Mamanguape; Mi = Miriri; Pb = Paraíba. White arrow = χ-anomaly. Dashed red line = lithological contacts between basement rocks (west) and sedimentary deposits (east). RDD = Regional drainage divide. Shaded relief based on SRTM-DEM. (b) SRTM-DEM 3D-view of an ongoing river capture between the upper Miriri River and a tributary of the Paraíba River left margin (vertical exaggeration = 30×). White dot in b = possible capture point.

Figure 11. Cross-divide statistics (average and standard deviation) and delta values based on Gilbert metrics and χ, including the estimated direction of the divide migration (see the location of divide segments in Figure 10a). (a) Channel elevation; (b) channel gradient; (c) relative relief at channel head. Red and black lines represent the sides of the drainage divides. The main geological units of each divide segment are presented on the top of the graph in a. Pb = Precambrian basement rocks; Pg = Paleogene unit; M = Miocene unit; Qa = Quaternary unit. (d) Normalized cross-divide delta values (c.f., Forte and Whipple, 2018) and uncertainties (standard deviation) for each of the four metrics derived from headwater channels, illustrating the stable and mobile divide segments in the passive continental margin.

Figure 12. Predicted average uplift rates for the Borborema Province in northeastern Brazil and palaeoelevation estimates for the central Andean Plateau. Black line and grey area with ±1 error band = average predicted uplift rates over the last 70 Myr based on inverse river profile modelling. Purple bar = palaeoelevation estimates (vertical axis to the left) over the past 30 Myr based on carbonate oxygen isotopes. The main phases of Andean orogeny are also indicated above the diagram (i.e., Peruvian: 80-65 Myr, Incaic: 45-28 Myr and Quechuan: 22-0 Myr). Uplift rate and palaeoelevation data simplified from Tribaldos et al. (2017) and Garzione et al. (2008), respectively. Phases of Andean Orogeny based on Coutand et al. (2001).

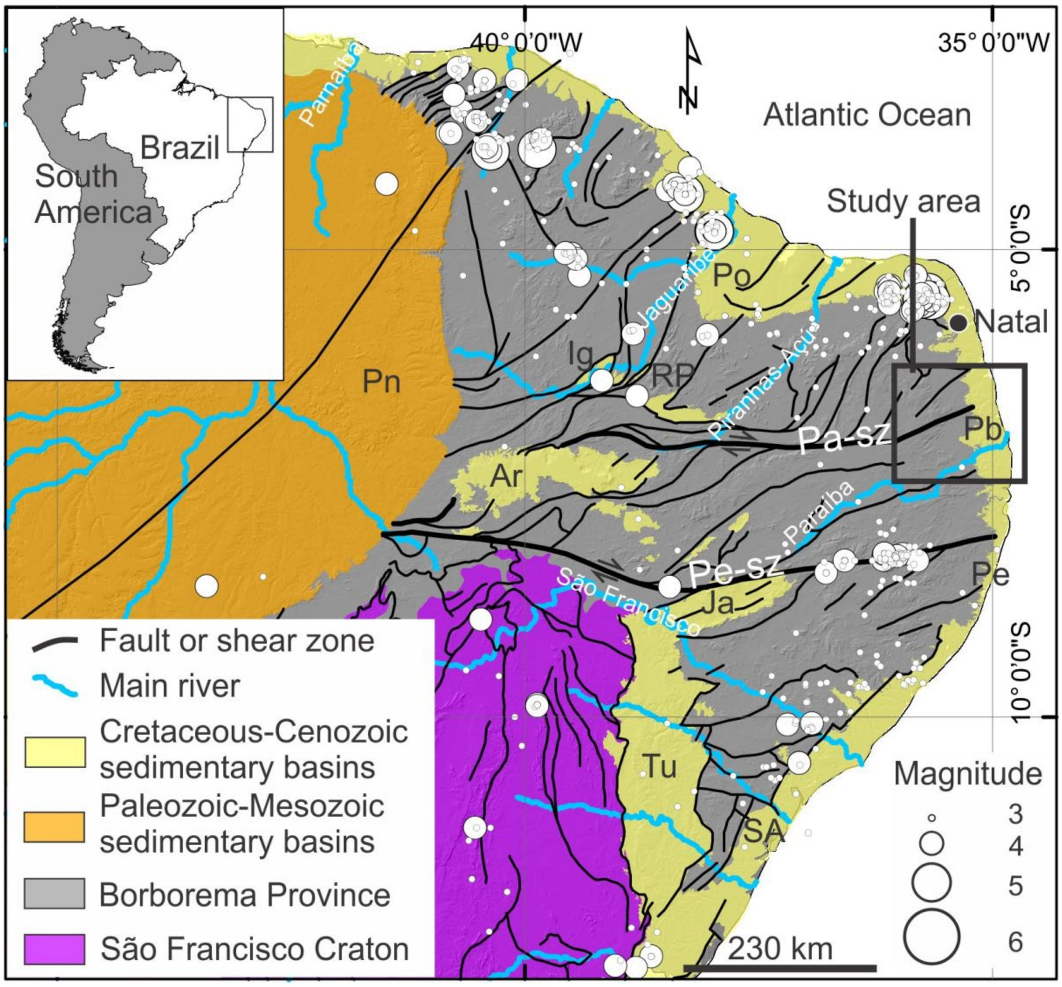
40° 0'0"W
35° 0'0"W
Atlantic Ocean
Study area
5°0'0"S
10°0'0"S
Natal
Brazil
South America
Parnaíba
Jaguaribe
Piranhas-Açu
Paraíba
São Francisco
Pn
Po
Ig
RP
Pa-sz
Pb
Ar
Pe-sz
Ja
Pe
Tu
SA
Fault or shear zone
Main river
Cretaceous-Cenozoic sedimentary basins
Paleozoic-Mesozoic sedimentary basins
Borborema Province
São Francisco Craton
Magnitude
3
4
5
6
230 km

Fig.1.

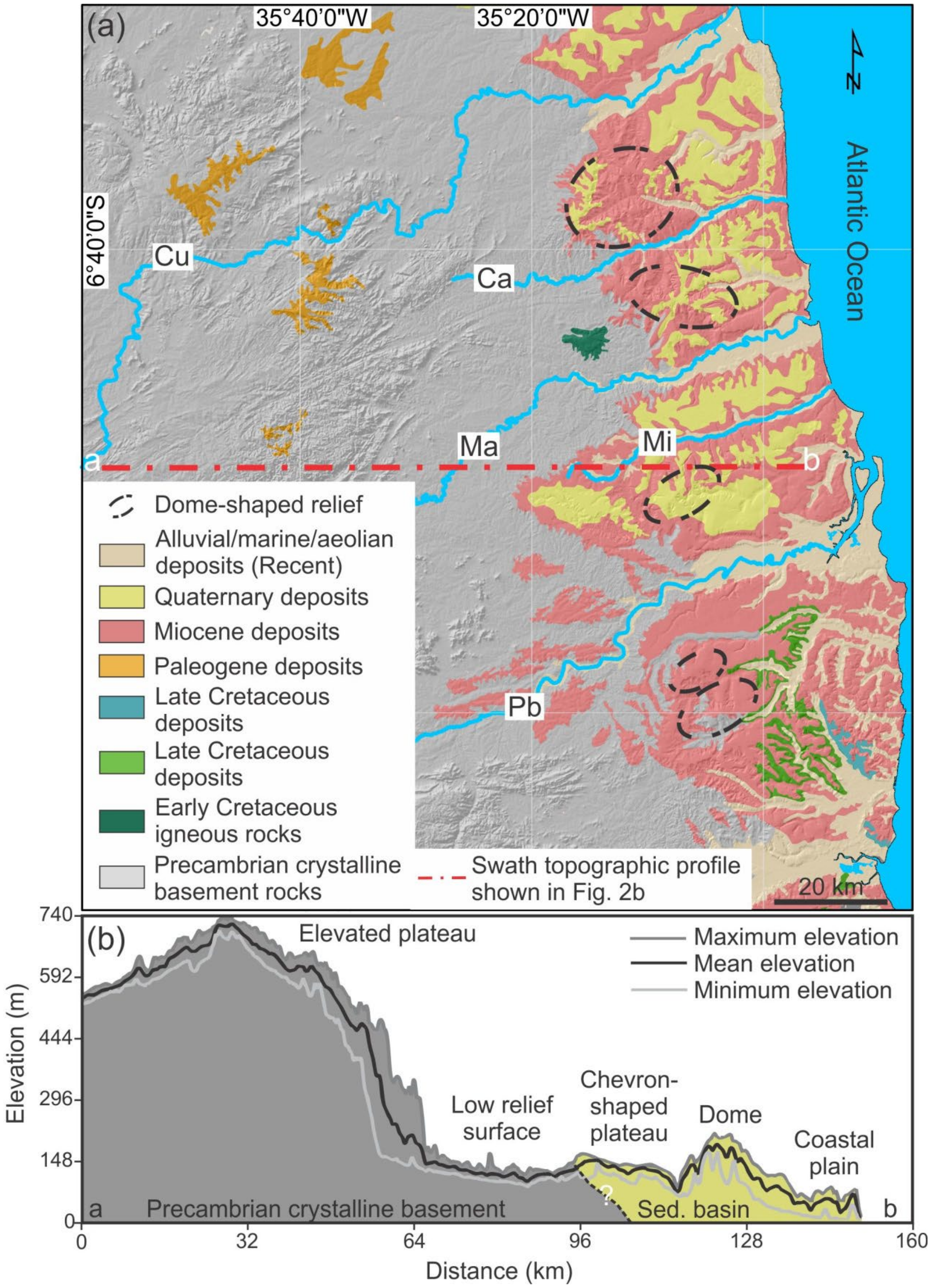
(a)
35°40'0"W
35°20'0"W
6°40'0"S
Atlantic Ocean
Cu
Ca
Ma
Mi
Pb
a
b
Dome-shaped relief
Alluvial/marine/aeolian deposits (Recent)
Quaternary deposits
Miocene deposits
Paleogene deposits
Late Cretaceous deposits
Late Cretaceous deposits
Early Cretaceous igneous rocks
Precambrian crystalline basement rocks
Swath topographic profile shown in Fig. 2b
20 km
(b)
Elevated plateau
Maximum elevation
Mean elevation
Minimum elevation
Low relief surface
Chevron-shaped plateau
Dome
Coastal plain
Precambrian crystalline basement
Sed. basin
?
Elevation (m)
740
592
444
296
148
0
Distance (km)
0
32
64
96
128
160

Fig.2.

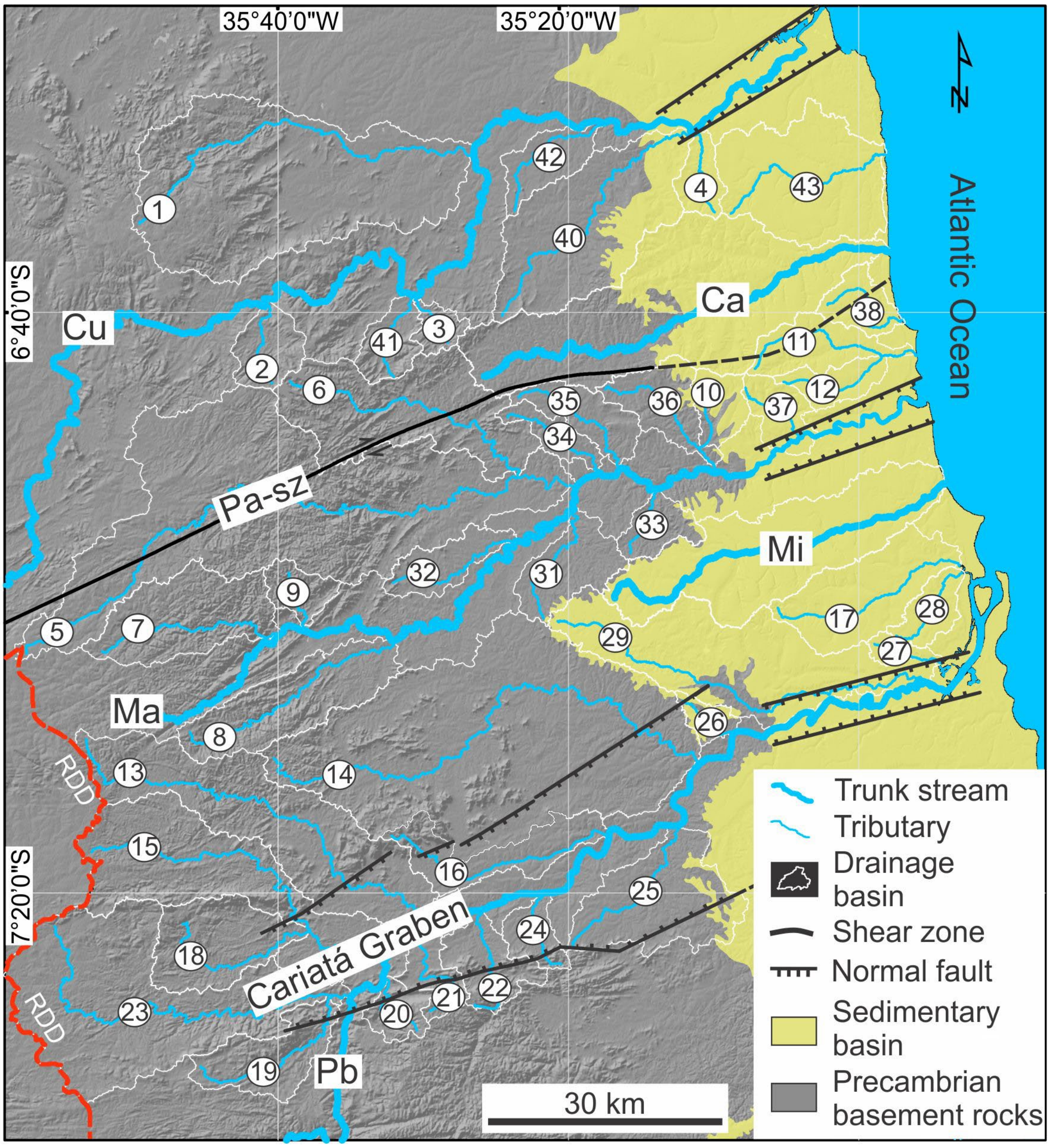
35°40'0"W
35°20'0"W
6°40'0"S
7°20'0"S
Atlantic Ocean
Cu
Ca
Mi
Ma
Pb
Pa-sz
Cariatá Graben
RDD
RDD
1
2
3
4
5
6
7
8
9
10
11
12
13
14
15
16
17
18
19
20
21
22
23
24
25
26
27
28
29
31
32
33
34
35
36
37
38
40
41
42
43
30 km
Trunk stream
Tributary
Drainage basin
Shear zone
Normal fault
Sedimentary basin
Precambrian basement rocks

Fig. 3.

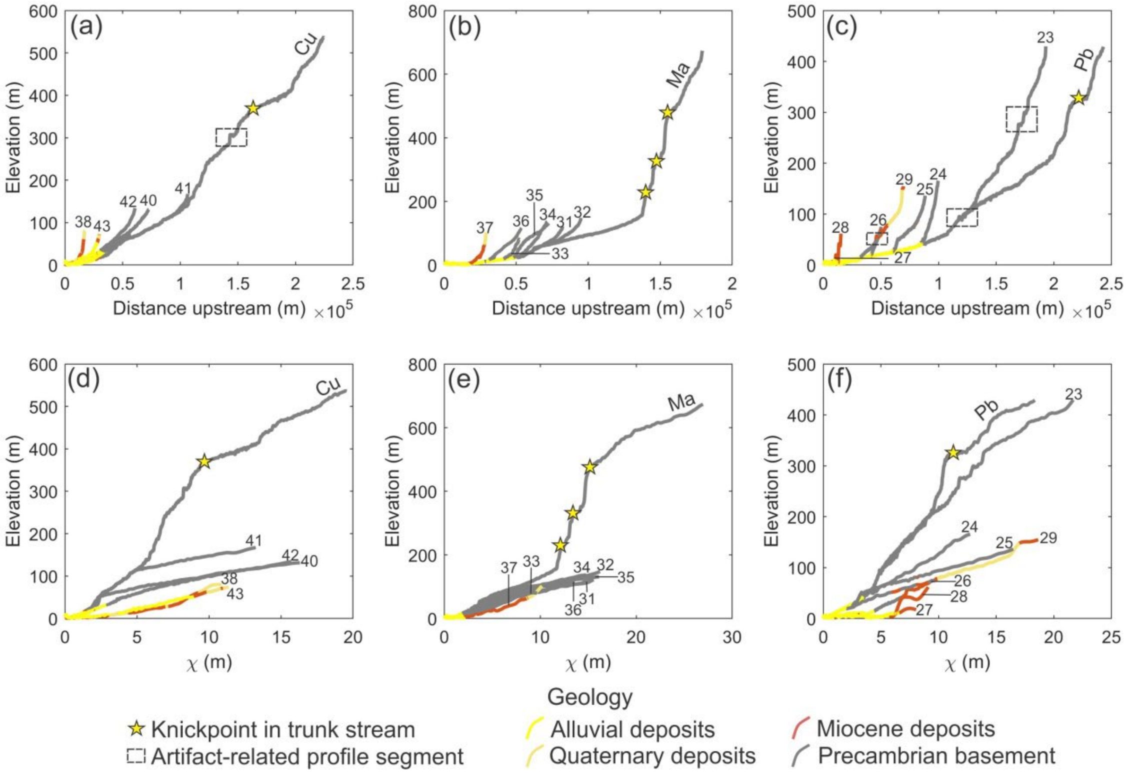
(a)
(b)
(c)
(d)
(e)
(f)
Elevation (m)
Distance upstream (m) ×10^5
χ (m)
Cu
Ma
Pb
Geology
Knickpoint in trunk stream
Artifact-related profile segment
Alluvial deposits
Quaternary deposits
Miocene deposits
Precambrian basement

Fig.4.

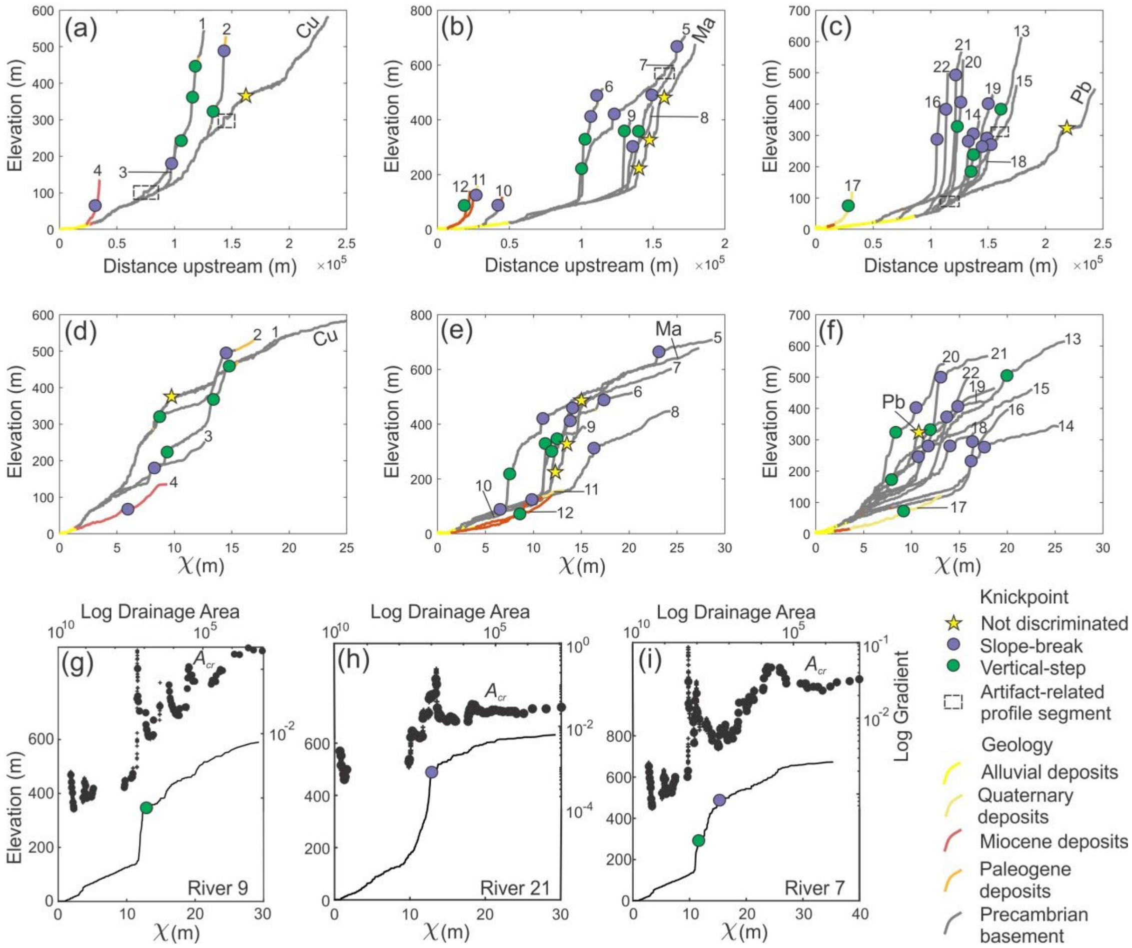
(a)
(b)
(c)
(d)
(e)
(f)
(g)
(h)
(i)
Elevation (m)
Distance upstream (m) ×10^5
χ(m)
Log Drainage Area
Log Gradient
A_cr
River 9
River 21
River 7
Knickpoint
Not discriminated
Slope-break
Vertical-step
Artifact-related profile segment
Geology
Alluvial deposits
Quaternary deposits
Miocene deposits
Paleogene deposits
Precambrian basement

Fig.5.

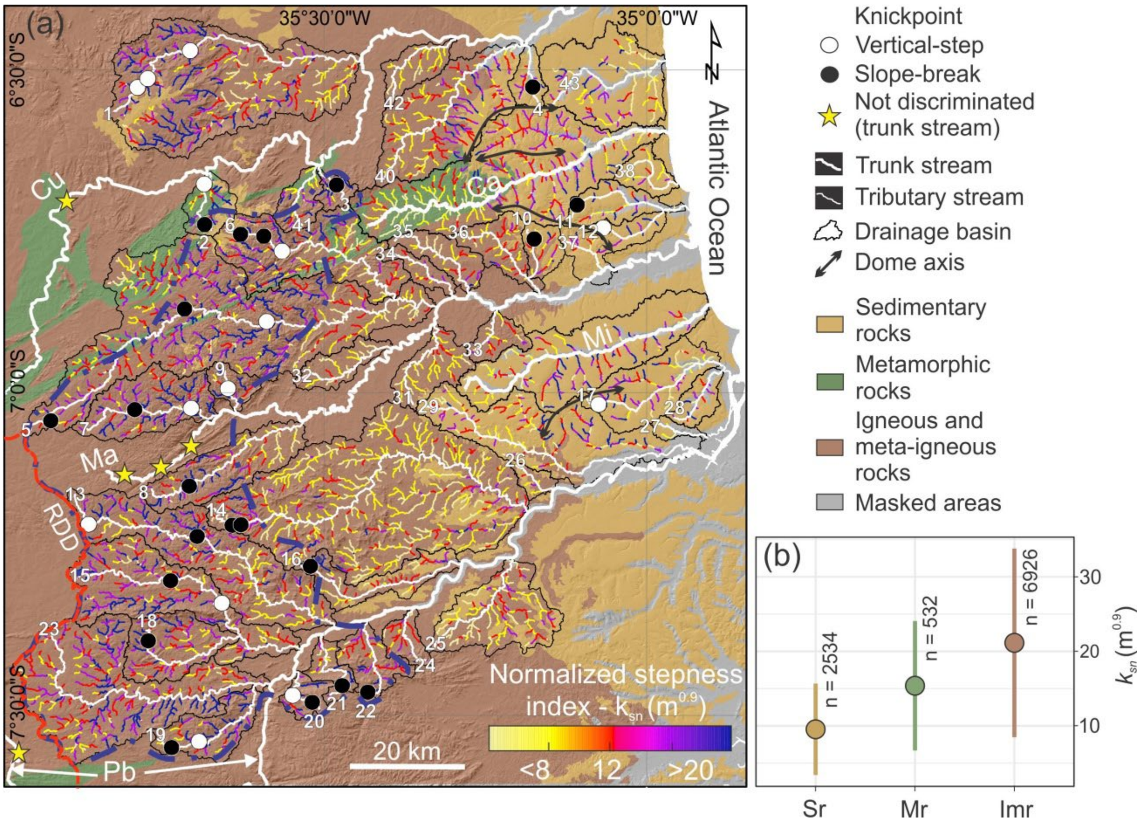

Fig.6.

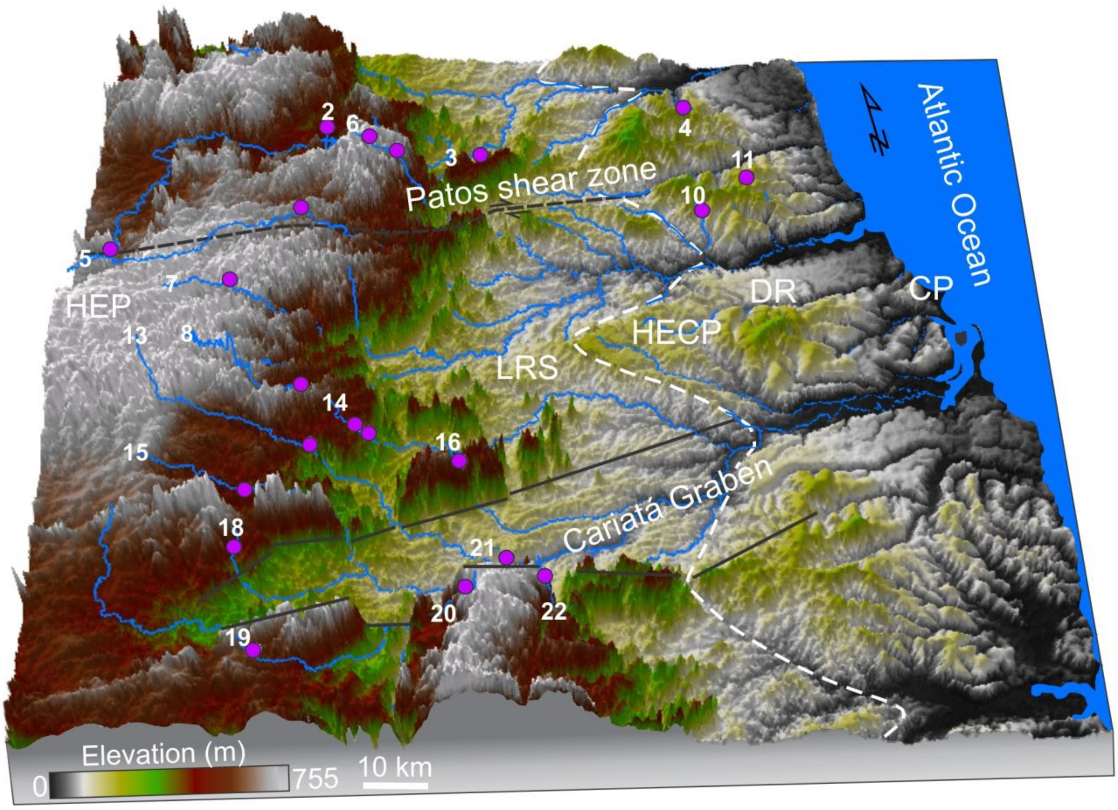

Fig.7.

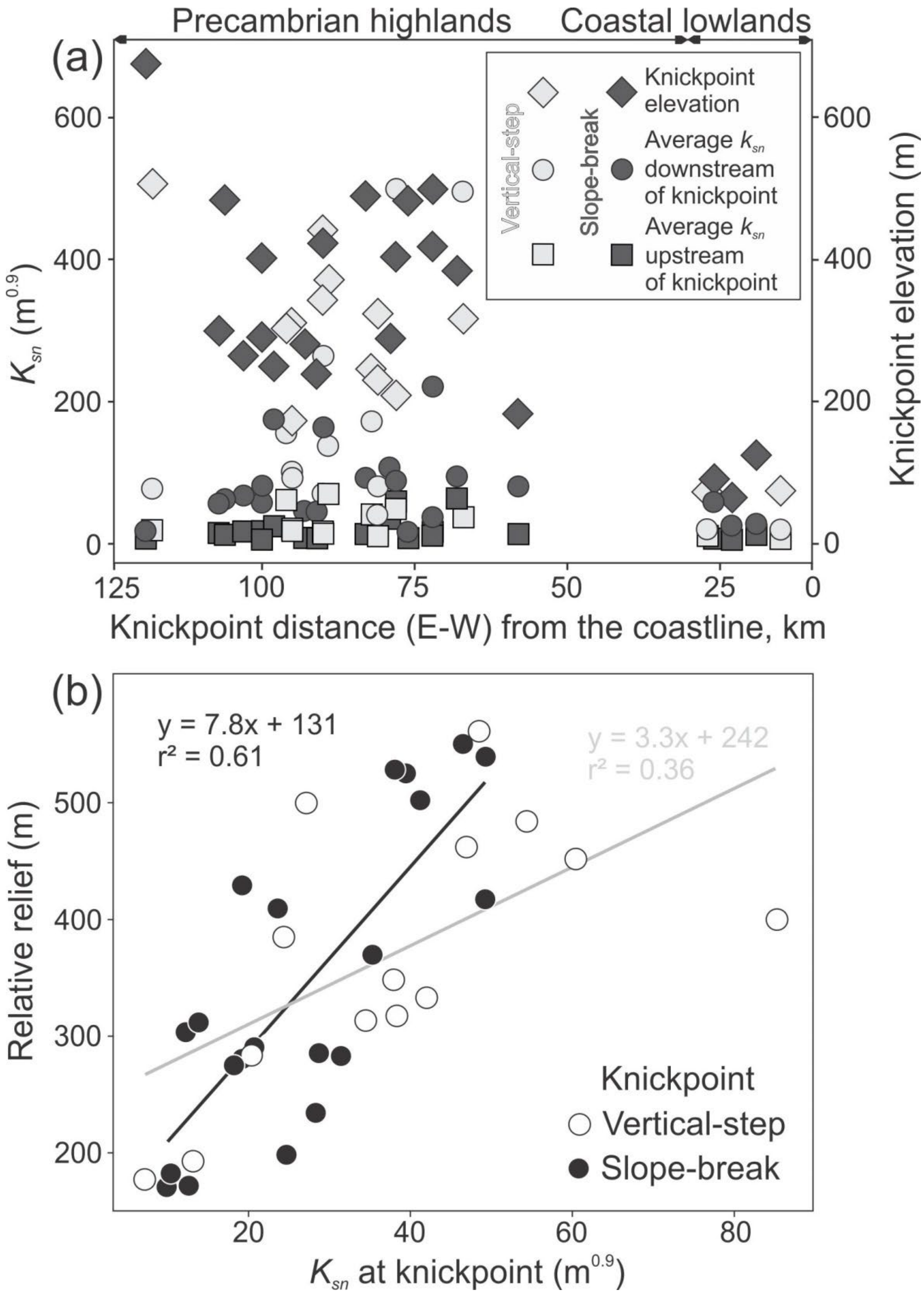
Precambrian highlands
Coastal lowlands
(a)
Vertical-step
Slope-break
Knickpoint elevation
Average k_{sn} downstream of knickpoint
Average k_{sn} upstream of knickpoint
K_{sn} ($m^{0.9}$)
Knickpoint elevation (m)
Knickpoint distance (E-W) from the coastline, km
(b)
y = 7.8x + 131
r² = 0.61
y = 3.3x + 242
r² = 0.36
Relative relief (m)
Knickpoint
Vertical-step
Slope-break
K_{sn} at knickpoint ($m^{0.9}$)

Fig.8.

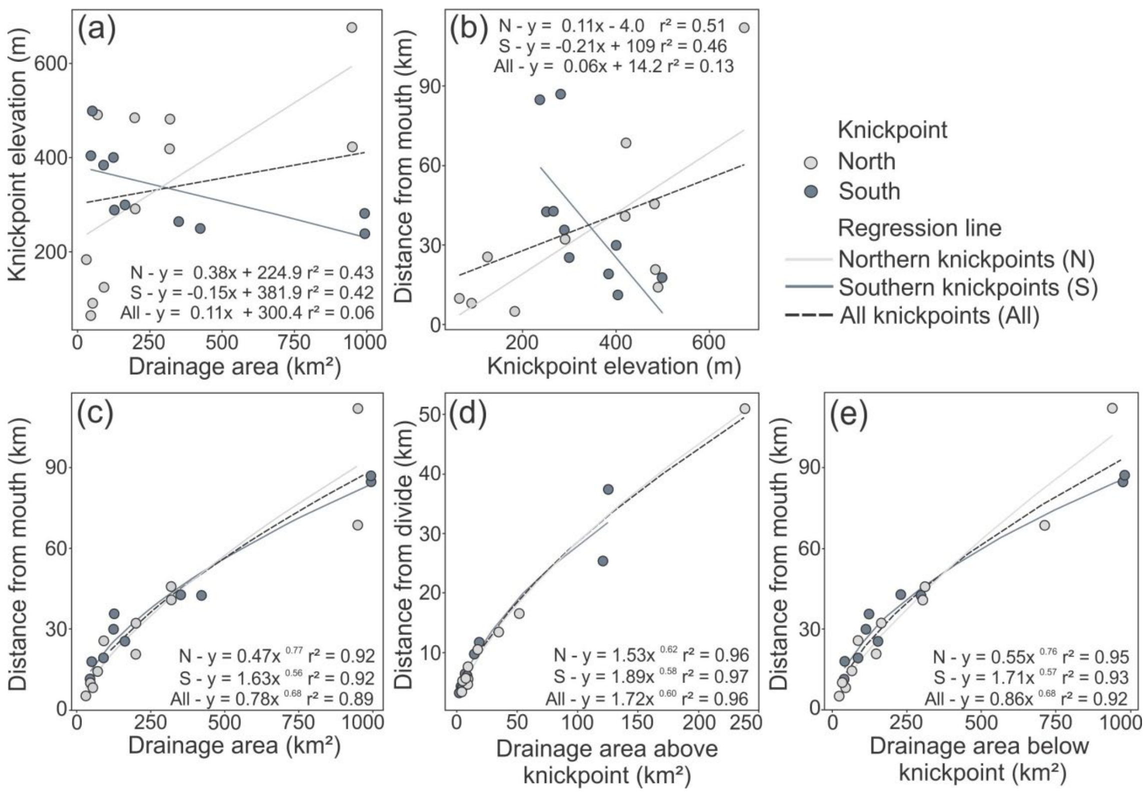

1325

1326 Fig.9.

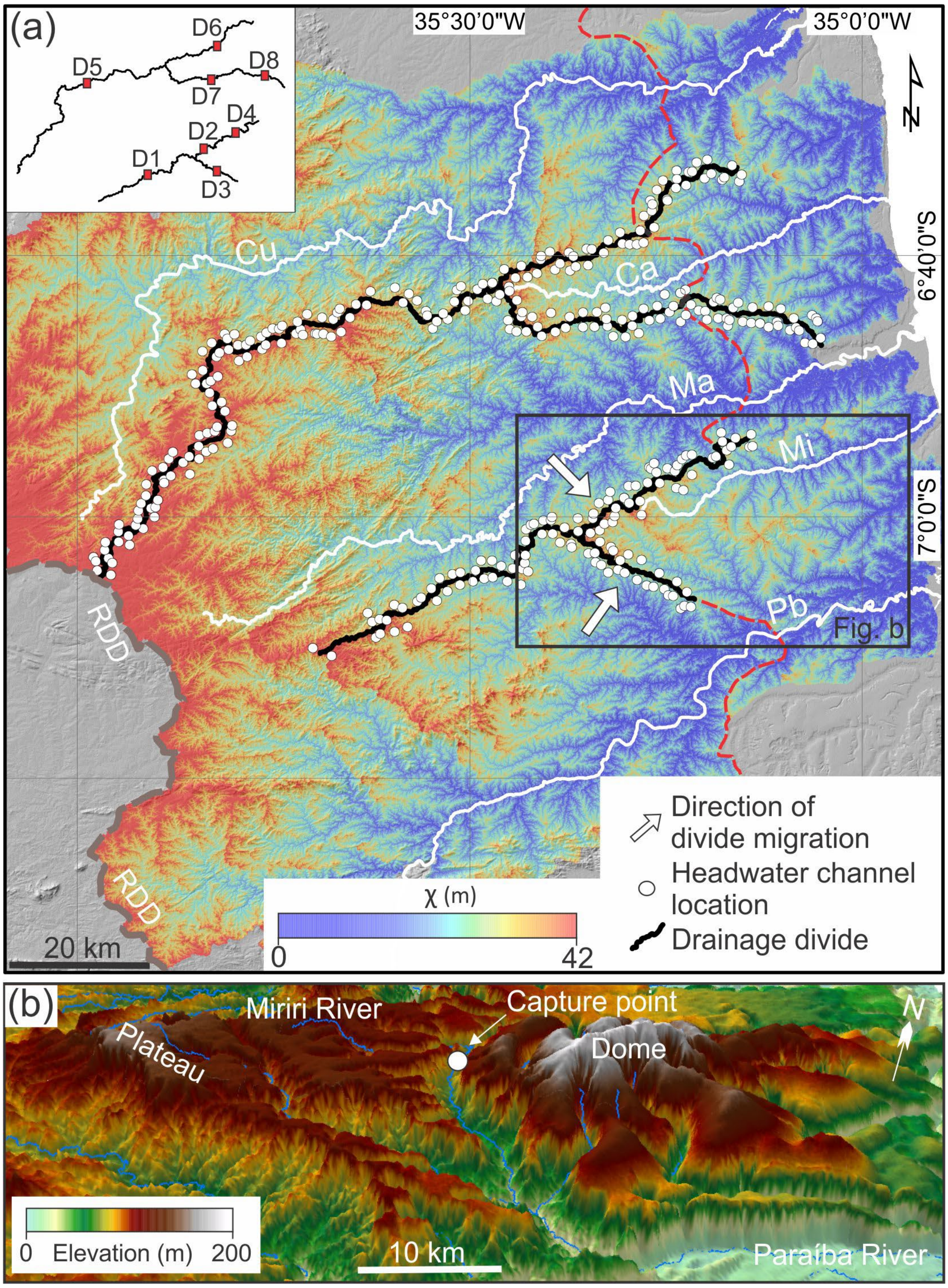

1327

1328 Fig.10.

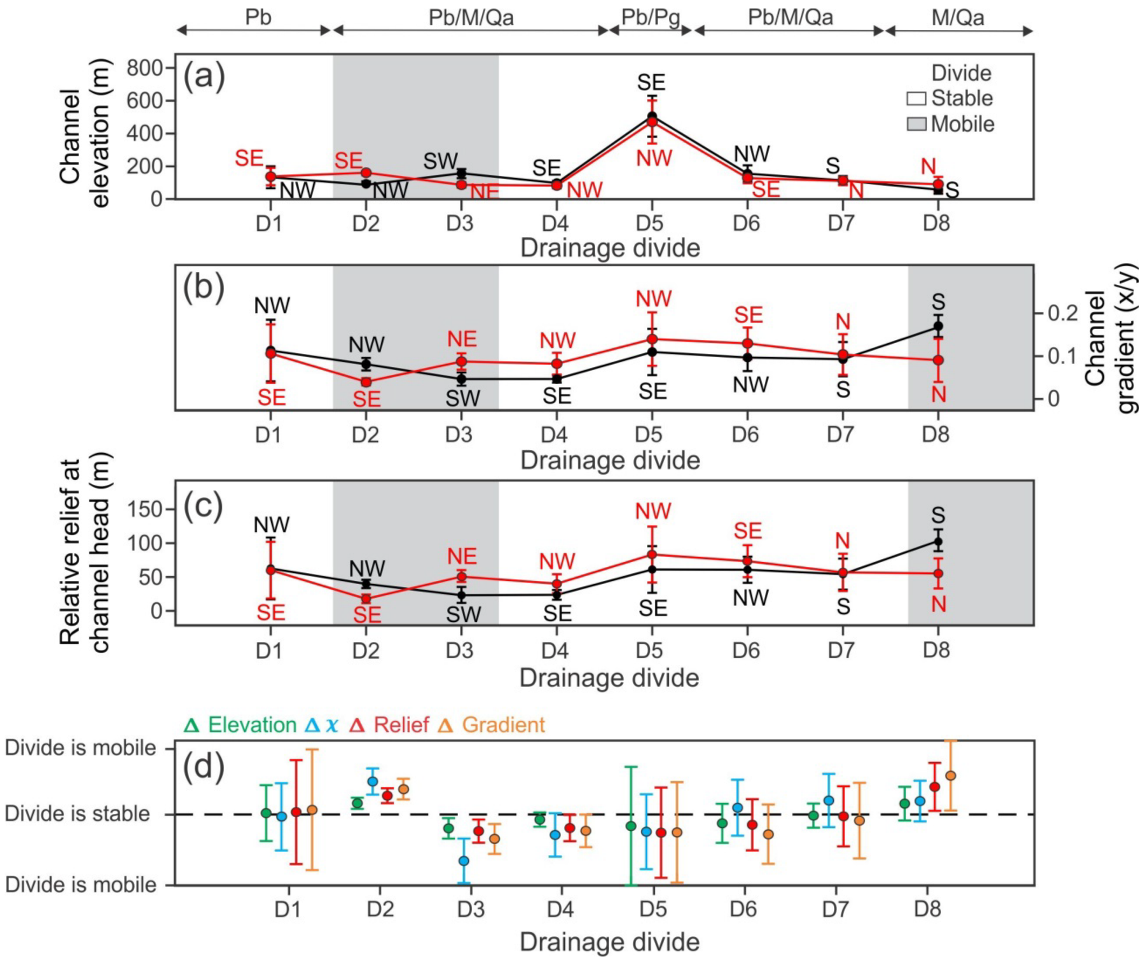

Pb
Pb/M/Qa
Pb/Pg
Pb/M/Qa
M/Qa
(a)
Channel elevation (m)
Divide
Stable
Mobile
Drainage divide
(b)
Channel gradient (x/y)
Drainage divide
(c)
Relative relief at channel head (m)
Drainage divide
Δ Elevation Δ χ Δ Relief Δ Gradient
(d)
Divide is mobile
Divide is stable
Divide is mobile
Drainage divide

Fig.11.

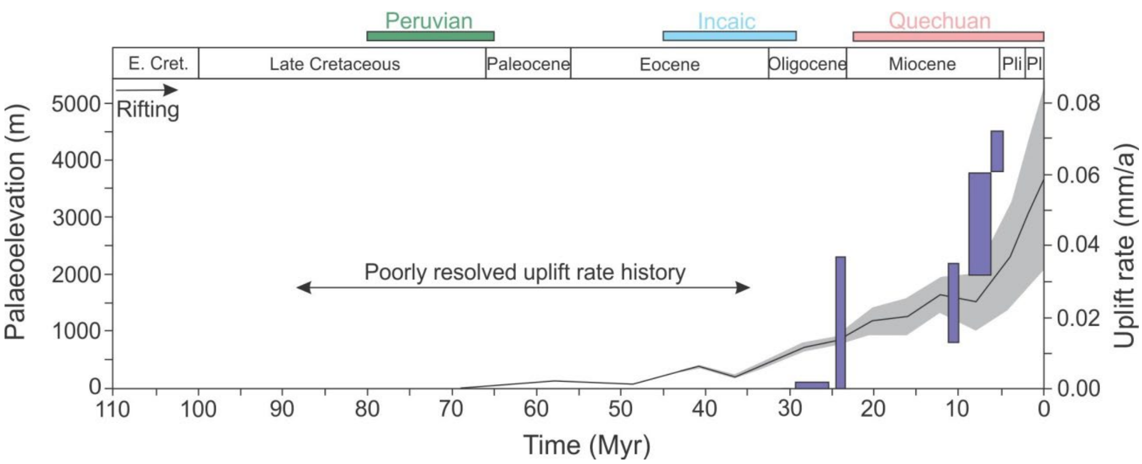

Peruvian
Incaic
Quechuan
E. Cret.
Late Cretaceous
Paleocene
Eocene
Oligocene
Miocene
Pli
Pl
Rifting
Poorly resolved uplift rate history
Palaeoelevation (m)
Uplift rate (mm/a)
Time (Myr)

Fig.12.

Table 1. Summary of the main lithologies exposed in the study area, including their ages and groups according to their relative resistance to erosion.

Age	Main lithologies	Geological unit name	Relative resistance to erosion
*Quaternary	Sandstones	Post-Barreiras	Low resistant sedimentary rocks
Miocene	Sandstones and mudstones	Barreiras	
Paleogene	Sandstones	Serra do Martins	
Late Cretaceous	Sandstones and limestones	Beberibe and Gramame	
Early Cretaceous	Phonolith and rhyolite	Itapororoca	Igneous, more or less massive, highly resistant
Neoproterozoic	Schists	Seridó	Metamorphic rocks, moderately resistant
Neoproterozoic, Mesoproterozoic and Paleoproterozoic	Gneisses, Migmatites and Granites	Suíte Várzea Alegre, Serrinha - Pedro Velho - units 1-2-3-4, Cabaceiras, Salgadinho, Serra de Jabitacá, Sertânea, Recanto - Riacho do Forno, São Caetano and Campina Grande, Esperança, Monte de Gameleiras, Serra Redonda, São Lourenço, Sumé, and Dona Inês and Caxexa plutons	Igneous and meta-igneous, more or less massive, highly resistant

* after Rossetti et al. (2012).

Table 2. Summary of the main characteristics of tributary streams bounded by knickpoints (slope-break and vertical-step), including fluvial metrics and estimates of fluvial incision.

River number	River length (km)	Drainage area (km²)	Elev (m)	Dfm (km)	Dfd (km)	Area up (km²)	Area down (km²)	K_{sn} up ($m^{0.9}$)	±	K_{sn} down ($m^{0.9}$)	±	K_{sn} at kp ($m^{0.9}$)	K_{sn} ratio	Fluvial incision (m)
Slope-break knickpoint														
2	16.0	70.6	490	14.2	3.4	4.2	66.4	13.7	0.5	92.3	2.7	12.3	6.7	135
3	9.9	30.7	183	5.0	5.7	7.3	23.4	13.2	0.8	80.2	4.1	13.8	6.1	45
4	13.7	46.5	65	10.0	5.4	9.4	37.1	4.8	1.7	24.6	1.2	12.6	5.1	20
5	117.4	950.6	676	112.0	7.5	9.5	941.1	6.7	0.1	18.2	0.1	24.7	2.7	100
5	117.4	950.6	423	68.6	51.0	238.3	712.3	18.2	0.1	163.6	16.3	28.3	9.0	60
6	48.8	319.4	483	45.7	5.7	7.4	312.0	7.8	0.3	17.0	0.9	19.2	2.2	370
6	48.8	319.4	419	40.8	10.5	17.3	302.1	17.0	0.9	36.5	1.7	41.2	2.1	270
7	33.9	198.9	484	20.6	16.5	51.6	147.3	12.2	0.1	61.9	1.5	31.4	5.1	180
8	43.2	200.1	291	32.2	13.4	34.8	165.3	17.6	0.3	58.6	0.7	49.2	3.3	110
10	16.0	53.3	91	8.2	4.7	8.8	44.5	7.1	0.4	58.9	4.1	9.9	8.3	50
11	28.8	92.0	125	25.6	5.2	5.2	86.8	12.4	0.7	27.7	2.3	10.4	2.2	60
13	77.9	422.3	250	42.6	37.4	125.3	297.0	24.6	0.2	174.3	7.5	35.3	7.1	75
14	94.0	993.8	281	86.8	9.7	14.7	979.1	7.6	0.1	45.4	1.4	28.7	5.9	112
14	94.0	993.8	239	84.8	11.7	18.7	975.1	7.6	0.1	45.4	1.4	22.6	5.9	90
15	64.9	349.3	265	42.7	25.4	120.8	228.5	17.1	0.2	67.2	2.9	19.2	3.9	80
16	38.0	126.4	289	35.6	4.2	3.6	122.8	35.4	0.8	106.7	10.3	23.6	3.0	150
18	29.3	162.9	300	25.3	6.2	7.7	155.2	15.1	0.7	55.9	3.2	38.1	3.7	115
19	33.7	123.4	401	29.9	6.1	8.6	114.9	6.3	0.3	81.5	4.0	20.8	13.0	240
20	13.4	46.5	404	11.2	4.0	4.8	41.7	59.0	4.7	88.1	8.8	46.5	1.5	280
21	22.0	51.2	499	17.9	6.4	6.9	44.3	16.1	0.6	220.8	10.9	49.3	13.7	290
22	20.4	89.3	384	19.1	3.2	2.4	86.9	63.3	2.0	94.1	3.1	39.4	1.5	120
Vertical-step knickpoint														
1	64.7	666.4	442	56.7	9.7	32.6	633.8	17.3	0.2	70.8	3.6	38.3	4.1	
1	64.7	666.4	371	54.0	12.4	39.5	626.9	70.8	3.6	137.8	6.0	42	1.9	
1	64.7	666.4	231	40.7	25.7	121.7	544.7	20.7	0.2	81.5	7.7	37.9	3.9	
2	16.0	70.6	324	4.5	13.2	63.8	6.7	10.5	0.3	40.4	2.4	34.5	3.8	
5	117.4	950.6	209	44.5	75.0	408.9	541.7	48.5	1.3	498.2	15.8	85.3	10.3	
6	48.8	319.4	317	35.5	15.8	38.8	280.6	36.5	1.7	494.5	16.6	46.9	13.5	
7	33.9	198.9	304	7.6	29.6	173.4	25.5	61.9	1.5	155.2	6.8	60.4	2.5	
9	10.2	46.8	342	5.9	7.2	16.2	30.6	14.3	1.0	263.6	7.1	54.3	18.4	
12	16.7	51.6	75	14.3	4.5	3.1	48.5	6.9	0.9	19.2	0.7	7.2	2.8	
13	77.9	422.3	507	70.8	9.2	15.3	407.0	19.0	0.2	78.2	2.5	20.4	4.1	
15	64.9	512.1	174	25.6	42.5	261.5	250.6	21.0	0.3	101.0	5.2	27.1	4.8	
17	31.7	190.4	73	28.6	4.7	5.8	184.6	11.4	0.5	19.3	0.4	13.2	1.7	
19	33.7	123.4	311	24.3	11.7	36.9	86.6	18.0	0.5	93.1	9.6	24.3	5.2	
20	13.4	46.5	246	6.7	8.6	25.6	20.9	41.3	3.2	171.9	6.4	48.5	4.2	

Elev = Knickpoint elevation; Dfm = knickpoint distance from mouth; Dfd = Knickpoint distance from divide; Area up = drainage area upstream of knickpoint; Area down = drainage area downstream of knickpoint; k_{sn} up = k_{sn} upstream of knickpoint; k_{sn} down = k_{sn} downstream of knickpoint; k_{sn} at kp = k_{sn} at knickpoint.

Table 3. Summary of the unpaired two-samples T and Mann-Whitney U statistical tests comparing topographic parameters of slope-break knickpoints recorded in the northern (N) and southern (S) sectors of the studied passive continental margin.

Unpaired two-samples T-test

Topographic parameter	Sector	Average	Standard deviation	Shapiro-Wilk test: p-value	Levene test: p-value	Two sample t-test: t-statistic	Two sample t-test: p-value
Elevation	N	339.1	200.0	0.337	0.004	0.119	0.907
	S	331.2	85.5	0.168			
* Relative relief	N	139.1	41.9	0.471	0.003	-1.640	0.124
	S	186.7	82.5	0.098			
** Relative relief	N	208.5	66.8	0.575	0.013	-2.610	0.021
	S	326.3	128.0	0.223			
*** Relative relief	N	277.6	106.0	0.122	0.591	-3.060	0.006
	S	421.7	109.0	0.074			
K_{sn}	N	28.7	18.1	0.099	0.036	-1.630	0.124
	S	46.1	29.1	0.362			

Mann-Whitney U test

Topographic parameter	Sector	Median	Interquartile range			Mann Whitney test: W-statistic	Mann Whitney test: p-value
Slope	N	2.71	1.9	-	-	47	0.5965
	S	2.74	0.9	-	-		

Relative relief with window radius of 1 (*), 3 (**) and 5 km (***).